AGU PUBLICATIONS

JGR

Journal of Geophysical Research: Solid Earth

RESEARCH ARTICLE

10.1002/2014JB010953

Key Points:
- New tomographic images of the Pyrenees and Massif Central
- The deep Pyrenean architecture is segmented by NE-SW transfer zones

Correspondence to:
S. Chevrot,
sebastien.chevrot@irap.omp.eu

Citation:
Chevrot, S., et al. (2014), High-resolution imaging of the Pyrenees and Massif Central from the data of the PYROPE and IBERARRAY portable array deployments, *J. Geophys. Res. Solid Earth*, *119*, doi:10.1002/2014JB010953.

Received 13 JAN 2014
Accepted 11 JUL 2014
Accepted article online 28 JUL 2014

High-resolution imaging of the Pyrenees and Massif Central from the data of the PYROPE and IBERARRAY portable array deployments

Sébastien Chevrot[1], Antonio Villaseñor[2], Matthieu Sylvander[1], Sébastien Benahmed[1], Eric Beucler[3], Glenn Cougoulat[4], Philippe Delmas[1], Michel de Saint Blanquat[5], Jordi Diaz[2], Josep Gallart[2], Franck Grimaud[1], Yves Lagabrielle[6], Gianreto Manatschal[7], Antoine Mocquet[3], Hélène Pauchet[1], Anne Paul[4], Catherine Péquegnat[4], Olivier Quillard[3], Sandrine Roussel[4], Mario Ruiz[2], and David Wolyniec[4]

[1]Observatoire Midi Pyrénées, IRAP, CNRS UMR 5277, Université Paul Sabatier, Toulouse, France, [2]Institute of Earth Sciences Jaume Almera, ICTJA-CSIC, Lluis Sole i Sabarís, Barcelona, Spain, [3]Observatoire des Sciences de l'Univers Nantes-Atlantique, Laboratoire de Planétologie et Géodynamique, CNRS UMR 6112, Université de Nantes, France, [4]ISTerre, Université Grenoble Alpes, CNRS UMR5275, Grenoble, France, [5]Observatoire Midi Pyrénées, GET, CNRS UMR 5563, Université Paul Sabatier, Toulouse, France, [6]Géosciences Rennes, CNRS UMR 6118, Université de Rennes 1, Rennes, France, [7]Institut de Physique du Globe de Strasbourg, EOST, Université de Strasbourg, Strasbourg, France

Abstract The lithospheric structures beneath the Pyrenees, which holds the key to settle long-standing controversies regarding the opening of the Bay of Biscay and the formation of the Pyrenees, are still poorly known. The temporary PYROPE and IBERARRAY experiments have recently filled a strong deficit of seismological stations in this part of western Europe, offering a new and unique opportunity to image crustal and mantle structures with unprecedented resolution. Here we report the results of the first tomographic study of the Pyrenees relying on this rich data set. The important aspects of our tomographic study are the precision of both absolute and relative traveltime measurements obtained by a nonlinear simulated annealing waveform fit and the detailed crustal model that has been constructed to compute accurate crustal corrections. Beneath the Massif Central, the most prominent feature is a widespread slow anomaly that reflects a strong thermal anomaly resulting from the thinning of the lithosphere and upwelling of the asthenosphere. Our tomographic images clearly exclude scenarios involving subduction of oceanic lithosphere beneath the Pyrenees. In contrast, they reveal the segmentation of lithospheric structures, mainly by two major lithospheric faults, the Toulouse fault in the central Pyrenees and the Pamplona fault in the western Pyrenees. These inherited Hercynian faults were reactivated during the Cretaceous rifting of the Aquitaine and Iberian margins and during the Cenozoic Alpine convergence. Therefore, the Pyrenees can be seen as resulting from the tectonic inversion of a segmented continental rift that was buried by subduction beneath the European plate.

1. Introduction

The opening and spreading of the Atlantic Ocean during the Cretaceous led to the breakup of the Laurasia supercontinent. The Bay of Biscay opened, and the Iberian plate separated and rotated with respect to the European plate. The convergence between Iberia and Europe, which led to the formation of the Pyrenees, started during the Campanian, around 80 Ma, and stopped around 30 Ma. Since then, Iberia has been part of the European plate and most of the convergence between Europe and Africa has been accommodated to the south of Iberia, in the Gibraltar Arc. The Pyrenean orogen is a continental double-wedge, with northward directed thrusts in the North and southward directed thrust in the South (Figure 1). It is divided into five units that are bounded by major faults: (1) The Aquitaine foreland basin, overthrust by (2) the North Pyrenean Zone (NPZ); (3) the Axial Zone of the chain, formed by Hercynian basement rocks; and (4) the South Pyrenean Zone (SPZ), which overthrusts (5) the Ebro foreland basin. The foreland basins developed on both sides of the Pyrenees in response to the flexure of the Iberian and European plates during the Pyrenean orogeny [e.g., *Brunet*, 1986]. Reflection profiles shot across the Pyrenees during the 1980s confirmed this general fan shape structure of the Pyrenean range [e.g., *Choukroune and the ECORS team*, 1989].

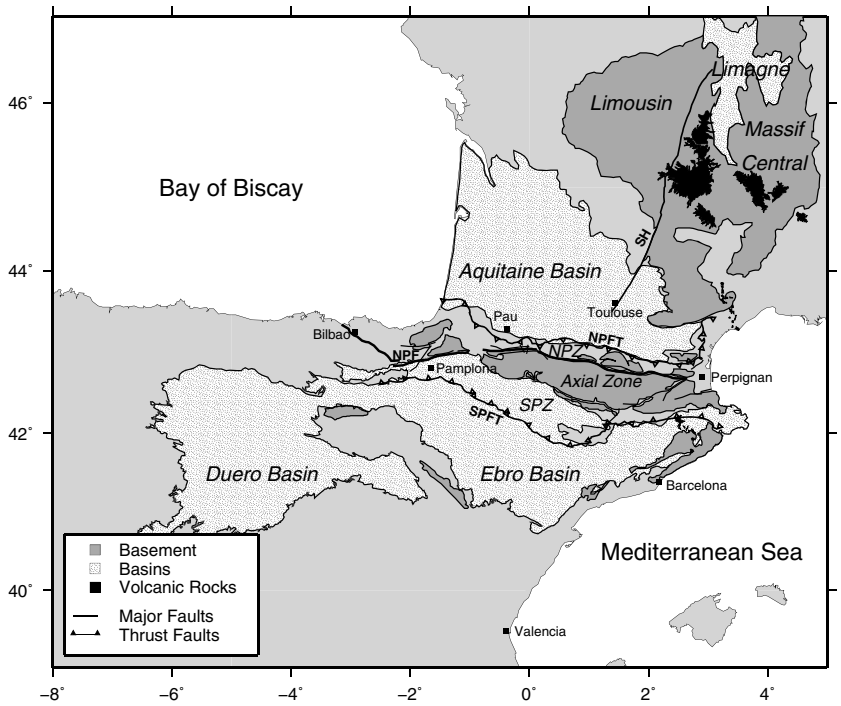

Figure 1. Main geological and structural units of the study region. NPF: North Pyrenean Fault, NPFT: North Pyrenean Front Thrust, SPFT: South Pyrenean Front Thrust, SH: Sillon Houiller (sometimes also referred to as the "Toulouse Fault"), NPZ: North Pyrenean Zone, and SPZ: South Pyrenean Zone.

1.1. A Problematic Plate Reconstruction

The geological history of the Pyrenees since the Mesozoic is tightly linked to the relative displacements of Iberia with respect to Europe. Two competing models have been proposed for the kinematics of the Iberian plate that produced the opening of the Bay of Biscay: (1) a scissors-type opening, with a pole of rotation located in the southeastern corner of the Bay of Biscay [e.g., *Sibuet et al.*, 2004] and (2) a left-lateral strike-slip opening, with a pole of rotation in the northwest of France [e.g., *Le Pichon et al.*, 1970, 1971]. These two models have been discussed in the literature ever since the 35° counterclockwise rotation of Iberia with respect to stable Europe was shown by a paleomagnetic study of igneous and sedimentary rocks from Portugal and Spain [*van der Voo*, 1969]. Since the 1970s and the first plate kinematic reconstructions, it is the second hypothesis that has been largely favored by both geologists and geophysicists, who first applied the newly developed concepts of plate tectonics to construct a model for the opening of the Atlantic Ocean and of the Bay of Biscay [*Le Pichon et al.*, 1970, 1971]. According to this model, during the Cretaceous, the North Pyrenean Fault (NPF) was a former transform plate boundary, along which transtensional pull-apart basins developed. The San Andreas Fault in Southern California would be a close modern analog to the NPF at that time [*Choukroune and Mattauer*, 1978].

However, more recent plate kinematic reconstructions found that a scissors-type opening of the Bay of Biscay provides a significantly better fit of the magnetic anomaly M0 [*Srivastava et al.*, 2000; *Sibuet et al.*, 2004]. These reconstructions imply that a relatively broad oceanic domain, up to 300 km wide, opened before the Aptian (113–126 Ma) between Iberia and Europe and was later closed by convergence during the Aptian while the Bay of Biscay was opening. The main problem with these models is that the closure of an oceanic domain would have left a suture to the south of the Pyrenees, as proposed in *Sibuet et al.* [2004], but none has ever been documented. In order to reconcile plate kinematic models with geological data, *Vissers and Meijer* [2012] proposed a new scenario in which around 300 km of a Neothetys ocean has been subducted beneath the Pyrenees. During the Albian (100–113 Ma), the subduction came to a halt and the gravitationally unstable slab detached, leading to extension and flysch deposition in the Pyrenean domain. In this model, the sinking of the detached lithosphere led to the ascent of asthenospheric mantle, responsible for the high-temperature metamorphism observed in the Pyrenees.

Since anomaly 34 (85 Ma), the convergence between Iberia and Europe is well constrained from plate kinematics. However, the rotation of Iberia and the opening of the Bay of Biscay occurred during the Cretaceous Normal Superchron. There is thus no seafloor anomaly to document intermediate stages between magnetic anomalies M0 (118 Ma) and 34 (85 Ma). In addition, the possibility to consider anomaly M0 as an isochron, which is implicit in plate reconstructions based upon the restoration of magnetic anomalies, is debated [*Bronner et al.*, 2011; *Tucholke and Sibuet*, 2012; *Bronner et al.*, 2012]. Therefore, the nature, timing, and localization of the relative movements of Iberia with respect to Europe currently remain highly uncertain.

1.2. The Pyrenean Domain During the Mesozoic

The nature of the Pyrenean domain during the Mesozoic, which is strongly related to the problem of the kinematics of the Iberian plate presented above, is also highly controversial. In the model proposed by *Choukroune and Mattauer* [1978] this domain was a wide strike-slip shear zone, characterized by E-W extension and small pull-apart basins. In this model the North Pyrenean Fault played a major role and corresponded to the former plate boundary.

This view has been challenged by some geologists who argued that there is a continuity of geological structures across the Pyrenees, which rules out any significant left-lateral movement of Iberia with respect to Europe after the Early Cretaceous [*Souquet and Mediavilla*, 1976]. In contrast, they proposed that the North Pyrenean Zone was a rift, segmented by NE-SW oriented faults. This rift hypothesis was later refined by *Boillot* [1986], who pictured the preserved Galicia margin as a modern analog of the Pyrenean rift, and explained the Pyrenean lherzolites by tectonic denudation of the mantle by lithospheric stretching associated to the rifting processes. This idea was revisited recently by *Lagabrielle and Bodinier* [2008] who attributed the emplacement of these lherzolites to mantle exhumation that occurred during an Albian strike-slip deformation linked to the rotation of Iberia. It is interesting to note that according to *Boillot* [1986], the strike-slip motion between Iberia and Europe occurs during the Albian and postdates the formation of the rift. The evolution of rift structures and their inversion during Pyrenean compression were reconsidered by *Jammes et al.* [2009]. They proposed that the prebreakup extension in the North Atlantic between Newfoundland and Iberia was of the order of 300–400 km and that this movement can account for most of the left-lateral displacement between Iberia and Europe. In this model, the eastward motion of Iberia occurred sometime between late Jurassic and late Aptian. The transtensional deformations were later overprinted by NE-SW rifting in the Pyrenean domain that resulted in major crustal thinning and mantle exhumation. In this latter model, rifting processes thus postdate the transtensional deformations. Hence, we see that the elusive kinematics of the Iberian plate during the Cretaceous allows very different interpretations of geological data, and while the extensional regime in the Pyrenees during the Albian/Aptian is now largely accepted, its global tectonic context is still very controversial.

1.3. A Poorly Constrained Pyrenean Convergence

Another way to constrain the relative movements between Iberia and Europe is to reconstruct the geological structures before the convergence and to quantify the amount of convergence that has been accommodated in the Pyrenean range. The exact amount of convergence is still debated, but minimum values ranging from 100 km [*Roure et al.*, 1989] to 147 km [*Muñoz*, 1992] have been proposed for the Central Pyrenees from a restored and balanced cross section along the ECORS seismic line. The main difference between these two reconstructions comes from different assumptions regarding the fate of the Iberian lower crust. According to *Roure et al.* [1989], the deep Iberian crust is currently stacked beneath the axial zone, while *Muñoz* [1992] favors continental subduction, with a minimum of 65 km of lower crust that has disappeared beneath the European crust, together with the Iberian lithospheric mantle. These two extreme models represent two possible interpretations of the ECORS seismic profile beneath the axial zone, simply because seismic reflectors in the deeper levels of the crust are poorly resolved. The shortening in the western Pyrenees is thought to be smaller than in the Central Pyrenees, of the order of 80 km, according to the restored crustal cross section made by *Teixell* [1998] along the ECORS-Arzacq reflection profile.

1.4. Previous Geophysical Studies

1.4.1. The Pyrenees

Early studies of critical reflections on the Moho from two fan profiles deployed in the central and eastern Pyrenees found that the Moho is offset vertically beneath the NPF by about 15 km in the Central Pyrenees [*Daignières et al.*, 1982]. This Moho step decreases toward the east, reaching a magnitude of only about 5 km

beneath the eastern Pyrenees while it is no longer observed beneath the Mediterranean Sea [*Gallart et al.*, 1980]. This result seemed to confirm the importance of the NPF, interpreted as the former plate boundary between Iberia and Europe.

In 1985 and 1986, Spanish and French organizations sponsored the ECORS-Pyrenees profile, the first seismic survey to cross an entire orogenic belt [*ECORS Pyrenees Team*, 1988; *McCaig*, 1988]. This experiment confirmed that the Iberian crust is thicker than the European crust, with a thickness of about 50 km south of the NPF. Deep reflectors beneath the NPF show that the Iberian crust underlies the southern edge of the European crust [*Choukroune and the ECORS team*, 1989], but the modeling of gravity anomalies suggests that the extension of the Iberian crust is less than 20 km north of the NPF [*Torné et al.*, 1989; *Daignières et al.*, 1989]. However, since the effects of metamorphic reactions on the density of subducted crustal material have been neglected in these studies, larger amounts of subduction cannot be excluded. Therefore, while the ECORS program has provided important first-order constraints on crustal structures in the Central Pyrenees, it certainly did not close the controversies on the deep lithospheric structures.

Regional *P* wave tomography, pioneered by *Aki et al.* [1977], is a powerful and yet simple approach to image lithospheric structures. During the last decades, it has been successfully applied worldwide in hundreds of different regions. Following the instrumental developments with ever increasing number of instruments deployed (sometimes up to a few hundreds), the resolution in resulting tomographic images has also improved dramatically, revealing lithospheric structures with more and more details. An earlier tomographic study of the Pyrenees [*Souriau and Granet*, 1995] suffered from the great heterogeneity and poor distribution of seismic stations, with a lack of stations in the center and at the western end of the range. The redeployment of permanent digital stations in 1996–1997 with a more even distribution of stations on both sides of the range somehow improved the ray coverage in a later tomographic study [*Souriau et al.*, 2008]. However, in this later study the overall poor quality of the manual picks and the very small N-S aperture of the seismological array still strongly limited the resolution in the deeper part of the model, leading to rather inconclusive results regarding the deep lithospheric structures beneath the Pyrenees. Nevertheless, an important result of this work was the demonstration that crustal structures can have a strong signature in tomographic images down to depths as large as 200 km, if not properly corrected for. Indeed, when accounting for the 15 km Moho offset at the NPF, the large low-velocity anomaly that was observed down to about 100 km depth in *Souriau and Granet* [1995], and interpreted as subducted Iberian crust [*Souriau and Granet*, 1995; *Vacher and Souriau*, 2001], completely disappeared. Another important finding was the absence of any continuous high-velocity anomaly all along the range, which seemed to rule out a large seafloor opening before the collision.

1.4.2. The Massif Central

While the Massif Central (Figure 1) is not our primary objective, our seismological data set can also provide crucial insights into the deep mantle structures beneath this region and in particular into their relations with recent volcanism. Reactivation of Hercynian fracture systems during the Cenozoic led to the formation of the Limagne graben, which is structurally connected with the Bresse and Rhine grabens, through a complex system of transform faults. The formation of this broad rift system is thought to be related to the compressional stresses originating from the Pyrenees and Alpine collision zones [e.g., *Tapponnier*, 1977; *Ziegler*, 1992]. Simultaneously, Massif Central experienced an intense volcanism that is spatially and temporally correlated to the formation of the Limagne graben. Crustal thinning [*Perrier and Ruegg*, 1973], and volcanism, are limited to the east of the Sillon Houiller (also often referred to as the Toulouse fault), a major Variscan lithospheric fault [*Burg et al.*, 1990]. The Massif Central is characterized by a large negative Bouguer anomaly of about −70 mGal [*Perrier and Ruegg*, 1973], which requires the presence of a low-density body at around 50 km depth. Regional tomographic studies [*Granet et al.*, 1995a, 1995b] evidenced a broad (~200 km) low-velocity anomaly in the upper mantle from 250 km depth to the surface. They interpreted the low velocities in the lithosphere as produced by the remaining thermal signature of the magmas that percolated through the lithosphere. Below the lithosphere, the remnant of a plume-type structure would be responsible for the observed broad asthenospheric anomaly. Whether this plume has a deeper origin remains an open question.

1.5. Objectives and Outline

From this overview, we can conclude that after several decades of geological and geophysical studies, the opening of the Bay of Biscay and the formation of the Pyrenees are still debated. Controversies remain on the amount of convergence that has been accommodated in the Pyrenees, on the variations of the

convergence rate along the range, and on the amount of Iberian lithosphere subducted beneath the European plate (if any). Crucial constraints will come from the deep structures beneath the Pyrenees, which remain poorly known.

Here we exploit the data of the PYROPE and IBERARRAY experiments that were deployed simultaneously on both sides of the Pyrenees in order to obtain a tomographic model of *P* wave velocity down to 900 km depth. This paper is organized as follows. In section 2, we give a short description of the PYROPE and IBERARRAY experiments, and of the different permanent arrays from which we have collected seismological data. Section 3 presents the procedures to select data and measure accurately *P* and PKP traveltimes. Section 4 details the construction of the crustal model that we use to compute accurate crustal corrections. We demonstrate the importance of these crustal corrections, especially in the Pyrenees, where strong and sharp lateral variations of crustal thickness are observed. The final tomographic model, which reveals the deep structures beneath the Pyrenees and Massif Central with unprecedented detail, is presented in section 5. Special care has been taken in quantifying both the lateral and vertical resolution in this model. Finally, section 6 contains some preliminary interpretations of our tomographic model.

2. The PYROPE and IBERARRAY Experiments

Imaging the deep lithospheric structures beneath the Pyrenees implies a cross-border project, which inevitably complicates the seismological deployment and the data exchange. This was especially true for the two dense profiles deployed across the Pyrenees, which were effectively deployed and maintained by two different groups on each side of the border.

The TOPOIBERIA project which officially started in 2007 has a strong seismological component, the IBERARRAY network (http://iberarray.ictja.csic.es/) that has covered the entire Iberian Peninsula in three successive deployments, from south to north. Soon after the beginning of this project, the French seismological community mobilized in order to seize the unique opportunity to deploy a temporary array of broadband stations in the south of France, and around the Bay of Biscay, that would be synchronized with the beginning of the third IBERARRAY deployment, in the north of Iberia. This project, named PYROPE (http://w3.dtp.obs-mip.fr/RSSP/PYROPE), is funded by the French Agence Nationale de la Recherche (ANR) and officially started in September 2009, for a duration of 4 years. The backbone of the IBERARRAY and PYROPE experiments is constituted of a total of around 130 broadband stations. In addition, two dense profiles of medium band stations have been deployed across the Pyrenees. The first profile, in the central Pyrenees, approximately follows the ECORS line. The second profile, in the western Pyrenees, follows a line going approximately from Pamplona to Mont-de-Marsan. Both profiles were operational during approximately a year. The main objective of these dense profiles is to obtain refined constraints on the geometry of deep lithospheric structures beneath the Pyrenees. The additional motivation to deploy them along previous long range seismic profiles was to compare the potential of passive versus active imaging techniques and take advantage of their complementarity.

The temporary deployments are complemented by the permanent broadband stations of the Réseau Large Bande Permanent (RLBP—http://rlbp.unistra.fr) and short-period stations of the Réseau National de Surveillance Sismique (RéNaSS—http://renass.unistra.fr) on the French side and by the permanent broadband stations of the Instituto Geográfico Nacional (IGN—http://www.ign.es) and of the Institut Cartogràfic i Geològic de Catalunya (ICGC—http://www.icgc.cat/). Figure 2 shows a map of all the stations from which we collected data for the present study.

3. Construction of the Traveltime Database

Resolution in traveltime tomography is mainly controlled by ray coverage and errors of arrival time picks. It is therefore important to construct the most complete data set possible, make a careful data selection, and perform very accurate measurements.

3.1. Waveform Data

We complemented the PYROPE and IBERARRAY arrays with all the operational seismological stations in the study region, on both sides of the Pyrenees. We collected data from permanent and temporary velocimetric stations. On the French side, we collected data from the Réseau National de Surveillance Sismique

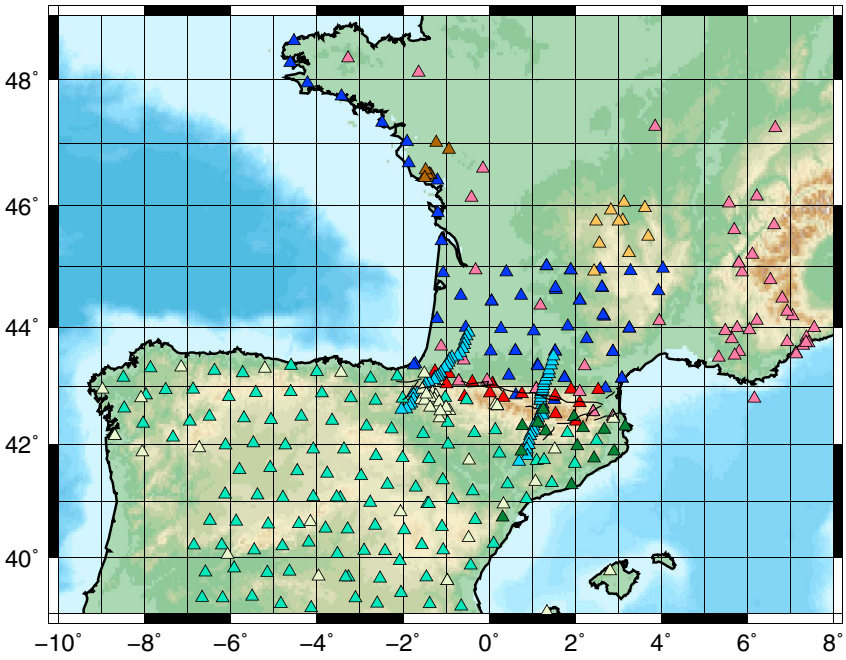

Figure 2. Map of the stations used in this study. We collected data from the RéNass in the Pyrenees (red triangles) and in the Massif Central (orange triangles), from the RLBP (pink triangles), from the ICGC (dark green triangles), and from a temporary experiment in Vendee (brown triangles) to complement the PYROPE (light and dark blue triangles) and IBERARRAY (light yellow and green triangles).

(RéNaSS—http://renass.unistra.fr) that operates 15 short-period stations in the Pyrenees (red triangles in Figure 2) and 10 short-period stations in the Massif Central (orange triangles in Figure 2).

We extracted all the available *P* or PKP vertical component seismograms produced by teleseismic events with a moment magnitude larger than 5.8 recorded by both permanent and temporary stations from January 2008 to September 2013. The data used in this study combine both broadband and short-period records, standardized to a WWSSN short-period instrument (peaked around 1 s). We select a time window on each record starting 5 s before and ending 10 s after the theoretical arrival time of the first arrival (the *P* or the PKPdf phase), computed in the ak135 reference Earth model [*Kennett et al.*, 1995]. A typical teleseismic event is recorded by around 250 stations and sometimes up to more than 300. To analyze efficiently such a large data set, we have developed a MATLAB graphical interface, which automatizes most of the data processing steps.

3.2. Data Selection by Cluster Analysis

Once the signal windows are extracted, a cluster analysis is performed over the complete set of traces. The algorithm, taken from *Knuth* [1968], associates the seismic traces into a number of equivalence classes according to their correlation coefficients. Since teleseismic waves recorded by a regional array have similar waveforms, the main cluster contains all the exploitable traces that are similar to one another. All the traces that do not belong to this main cluster are rejected. They usually correspond to stations that are not operating correctly. This step is important, because it allows us to select data automatically, avoiding the need to visually inspect hundreds of traces for each event.

3.3. Measurements of Differential and Absolute Traveltimes

The waveform similarity of teleseismic waves, already exploited for data selection, is also used to accurately measure relative arrival times by cross correlation. The multichannel cross-correlation technique introduced by *VanDecar and Crosson* [1990] has been very popular to determine accurate relative arrival times of teleseismic waves recorded by regional arrays. However, this technique requires preliminary picks on each trace, a tedious process for dense arrays with many recording stations that can also be problematic to perform on noisy records. To keep the procedure automatic, we follow the approach of *Chevrot* [2002] which consists in

finding the average waveform recorded by the array and the time delays at each station that minimize the misfit function:

$$E = \sum_{i=1}^{N} \sum_{j=1}^{M} |d_i(t_j) - s(t_j - \tau_i)| \quad (1)$$

where d is the observed record at station i, s is the average waveform, and τ_i its delay at station i. Note that we use a L_1 norm to reduce the effects of strongly incoherent arrivals in the coda of the P wave. This minimization problem is solved by simulated annealing [*Kirkpatrick et al.*, 1983]. For more details on the algorithm we refer the reader to *Chevrot* [2002].

Once the minimum of (1) has been found after a few thousands iterations, which takes a few seconds of CPU time on a laptop, all the records can be aligned with the average or reference waveform. It is then easy to pick the onset of the P wave on the reference waveform, which has an extremely high signal-to-noise ratio. Using the time delays τ_i, we can then compute absolute arrival times on each trace. We thus measure both absolute and relative arrival times, with a precision comparable to measurements based on cross correlations. However, by solving the global minimization problem (1), we avoid getting trapped into secondary maxima of the correlation functions, as in the approach by *VanDecar and Crosson* [1990]. The traveltime residuals are computed by subtracting the theoretical traveltime computed in the ak135 reference Earth model from the absolute traveltime obtained by simulated annealing. For each event, we then determine and subtract the average traveltime residual from all the traveltime residuals obtained for this event in order to mitigate the contribution of structures outside the regional tomographic grid, a standard procedure in regional tomography [*Aki et al.*, 1977]. Finally, the traveltime measurements are scrutinized individually in order to identify and discard bad measurements. This final step is performed by interactive visualization tools that are built into the graphical interface. Three criteria are examined by the analyst to identify and discard unreliable measurements: the traveltime residual itself, the correlation coefficient between each trace and the reference waveform, and the map of traveltime residuals. While a poor correlation coefficient usually reflects a high level of noise on the record, the measured traveltime residual may be acceptable and coherent with those measured at adjacent stations. On the contrary, we sometimes observed large correlation coefficients with anomalously large traveltime residuals, resulting from a clock problem of the recording station. We also found that some stations had a vertical component with reversed sign, a problem that could be identified by generally smaller correlation coefficients for these stations. Once identified, these problematic traces are corrected, if possible. If not, then they are rejected by the analyst by a mouse selection.

Overall, it takes a couple of minutes to process an event recorded by about 250 stations. With this method, we are thus able to process efficiently extremely large data sets in order to obtain clean and high-quality arrival time measurements. Note that, as a byproduct, this method also isolates the reference wavelet, a necessary ingredient to compute finite-frequency kernels, and thus opens the way toward regional finite-frequency tomography.

After analyzing the whole data set, we kept 135 earthquakes from which a total of more than 34,000 P or PKPdf residuals were obtained.

3.4. Examples

The analysis revealed clear variations of P residuals as a function of the incoming direction of the teleseismic wavefront. We illustrate this variability below by showing the residual maps for two events coming from different backazimuths.

3.4.1. Residual Map for the 17 November 2011 Ecuador Event

Figure 3 shows the map of P residuals for the 17 November 2011 Ecuador event ($M_w = 5.9$, depth = 30 km), i.e., for a teleseismic P wavefront coming from the SW. The first striking feature of this map is the very high spatial coherence of the P residuals. To the north of the Pyrenees, the residuals are negative while they are slightly positive to the south. The limit between these two regions approximately corresponds to the NPF. In Spain, the residuals show a continuous decrease toward the west to reach a minimum in Galicia.

3.4.2. Residual Map for the 11 August 2012 Zagros event

Figure 4 shows the map of P residuals for the 11 August 2012 Zagros event ($M_w = 6.4$, depth = 11 km), i.e., for a teleseismic P wavefront coming from the E. This map differs strikingly from the previous one: the P residuals to the north of the Pyrenees are now strongly positive, while they are slightly positive to the south. A strong negative anomaly is observed in the French Basque country. The P residuals in Spain still show a continuous decrease but this time toward the south.

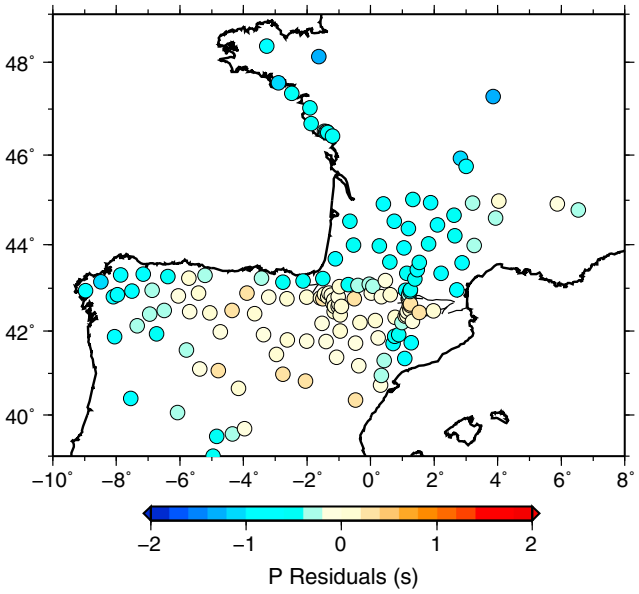

Figure 3. Map of *P* residuals for the 17 November 2011 Ecuador event.

4. Crustal Corrections

Crustal structures can introduce important biases in tomographic models. Indeed, owing to the subvertical incidence of teleseismic waves and the minimum L_2 norm constraint imposed to regularize the inversion that favors small values of velocity perturbations, crustal anomalies are smeared vertically in the tomographic model if not properly accounted for [e.g., *Waldhauser et al.*, 2002; *Li et al.*, 2006]. This problem is especially important in orogenic domains, where the crust can be thickened by up to 20 km (and sometimes even more like, for example, beneath the Tibetan plateau). Such a crustal thickening is equivalent to a velocity decrease of about 2% down to 200 km depth. Very thick sedimentary layers may also have a strong contribution to observed traveltime residuals.

While the computation of crustal corrections is straightforward, the problem is to have access to a detailed crustal model, able to provide accurate predictions of the crustal contribution to *P* wave delays. Global crustal models such as CRUST2.0 [*Bassin et al.*, 2000] are available, but in most places their accuracy is insufficient for this purpose. We found three regional crustal models published in the literature that cover our region of interest. The models by *Ziegler and Dèzes* [2006] and *Diaz and Gallart* [2009] rely on a compilation of information from deep seismic profiles, while the model by *Gómez-Ortiz et al.* [2011] has been derived from Bouguer anomalies. These three crustal models show some level of agreement, but they differ significantly on their estimates of the amplitude and lateral extent of the crustal roots beneath the Pyrenees and the Cantabrian Mountains. For example, the main crustal root in the central Pyrenees is at 42 km in the model by *Gómez-Ortiz et al.* [2011] while it is around 55 km in the model by *Ziegler and Dèzes* [2006], closer to the values reported by seismic reflection profiles studies [e.g., *Daignières et al.*, 1982, 1989]. However, the model by *Ziegler and Dèzes* [2006] show a normal crustal thickness in the Cantabrian Mountains, while the recent seismic profiles in that region have documented a clear crustal thickening, of about 10 km [*Pedreira et al.*, 2003; *Diaz and Gallart*, 2009]. In addition, since the construction of these maps of crustal thickness involved a significant amount of smoothing, their spatial resolution is insufficient to capture the strong and sharp variations of crustal thickness that are well documented beneath the Pyrenees. Since we expect the main crustal

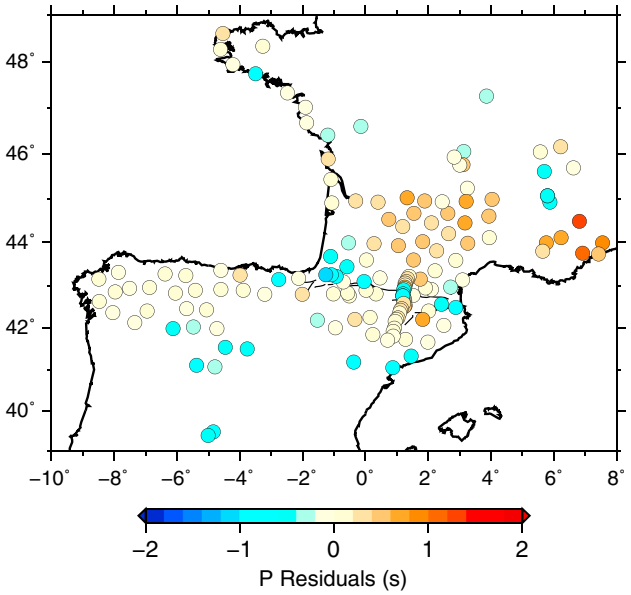

Figure 4. Map of *P* residuals for the 11 August 2012 Zagros event.

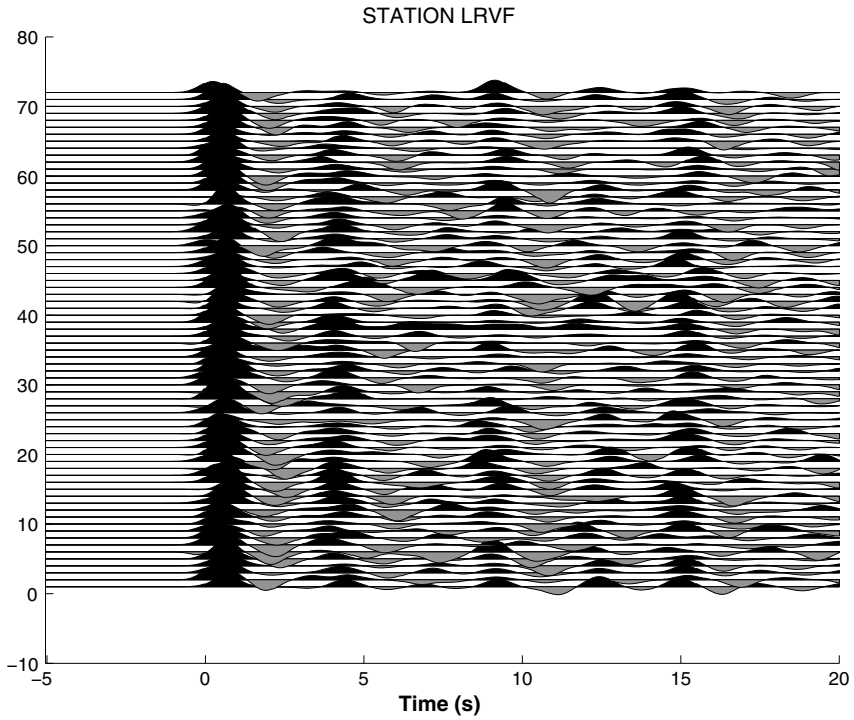

Figure 5. Receiver functions for permanent station LRVF (latitude 44.947°, longitude −0.312°).

signals to come from these orogenic regions, we have thus decided to construct a new and more refined crustal model.

There are different ways to construct crustal models: from the compilation of seismic reflection profiles [e.g., *Waldhauser et al.*, 2002; *Diaz and Gallart*, 2009], local tomographic studies [e.g., *Li et al.*, 2006], receiver functions, and gravity anomalies [e.g., *Gómez-Ortiz et al.*, 2011], to name a few. The regular spacing of seismological stations across the region opens the possibility to complement well the deep seismic soundings with receiver functions. The idea of this approach is to measure, at each station, the differential traveltime of the Pms phase (the *P* to *S* conversion at the Moho) with respect to the direct *P* wave. This time difference can then be converted to an apparent Moho depth in the reference model. It is then straightforward to compute the perturbation of the *P* wave traveltime produced by this perturbation of Moho depth. The advantage of this approach is that it avoids constructing a 3-D crustal velocity model. In addition, it provides accurate crustal corrections at the exact locations of seismological stations. Effects of lateral variations of crustal velocities are also naturally accounted for. For example, in a slower crust, the onset of the Pms will be shifted toward later arrival times. This will result in an apparently thicker crust and consequently in a larger crustal correction compared to a crust with a velocity close to normal.

Receiver functions are computed for the complete database of teleseismic events that has been gathered for the present tomographic study. We deconvolve the vertical components from the radial components using the iterative deconvolution method of *Ligorria and Ammon* [1999]. The receiver functions are then stacked, and we identify the largest peak in the stack between 2 s and 7 s after the *P* wave as the Pms phase. The processing has been automated, because we need to handle a very large number of seismological records. However, the stacks of receiver functions at each station are visually checked. Ambiguous results are discarded, and, if necessary, the identification of the Pms peak is manually updated. The main problem that we faced was the difficulty to exploit receiver functions for stations located in the Ebro and Aquitaine foreland basins. At almost all the stations in these basins, strong reverberations in shallow sedimentary layers masked conversion on deeper discontinuities, in particular, on the Moho. For example, for station LRVF (Figure 5), the receiver functions show a regular succession of reverberations with alternatively positive and negative amplitudes. This station is a permanent station installed in a cellar carved in solid rocks. The problem is thus not related to the quality of the installation but clearly to the local geological setting. Another problem

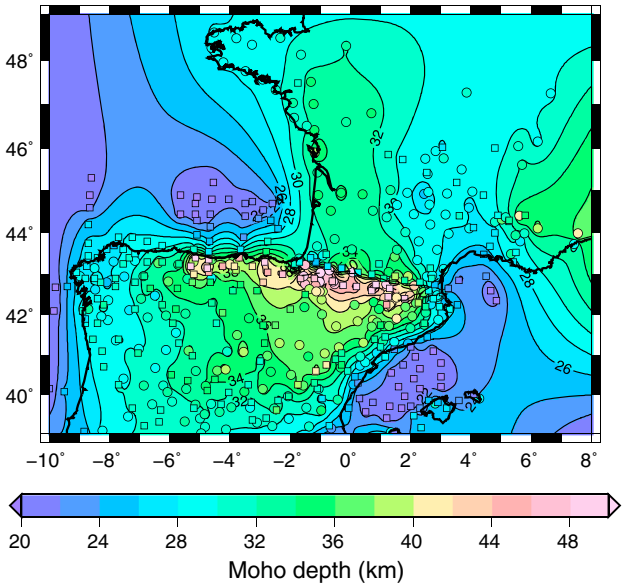

Figure 6. Map of crustal thickness. This map was obtained by interpolating the crustal thicknesses obtained from receiver functions (circles) and seismic reflection/refraction profiles (squares).

was the strong complexity and azimuthal variability of receiver functions inside the Pyrenean range, which sometimes hampered unambiguous identification of conversions on the Moho. For these stations, we resolved the ambiguity by choosing the conversion that gave a crustal thickness consistent with the one at adjacent stations. Obviously, more detailed images of crustal discontinuities could be obtained beneath the two dense profiles. These images will be presented and discussed in a forthcoming contribution, but the geometry of the Iberian and European Moho that come from the analysis of these two transects are in very good agreement with the regional crustal model detailed below.

Figure 6 shows the map of apparent crustal thickness that we derived from our receiver function analysis (circles) and from a compilation of reflection/refraction profiles in France [*Sapin and Prodehl*, 1973; *Sapin and Hirn*, 1974; *Perrier and Ruegg*, 1973; *Daignières et al.*, 1982] and Spain [*Diaz and Gallart*, 2009] (squares). To create this map, we have interpolated the crustal thickness over a regular 0.05° grid. Note the overall excellent agreement between the two types of constraints. The main features in the crustal map is the thickening of the crust beneath the Pyrenees, in particular, in its central part, where crustal thickness is larger than 55 km, and beneath the Basque-Cantabrian Mountains. The Massif Central is characterized by a thin crust, around 28 km thick. A thin crust is also observed along the western Galicia margin, as a result of the opening of the northern Atlantic Ocean. Crustal corrections computed in this crustal model are usually in the range ±0.3 s, which is significant.

5. The Tomographic Model

5.1. Inversion

The tomographic model is parameterized in a spherical grid with homogeneous blocks of dimension 0.25° in latitude and longitude and 25 km in depth down to 900 km depth. Rays are traced in the ak135 reference Earth model [*Kennett et al.*, 1995], and we compute the length of the rays inside all the blocks that are crossed. Following an algorithm similar to *Spakman and Bijwaard* [2001], we construct an irregular block model which agglomerates the small blocks of the initial regular grid in the poorly sampled parts of the model. This construction reduces the size of the inverse problem and improves its conditioning. To regularize the inversion, we add penalty conditions on the L_2 norm and Laplacian of the tomographic model. The tomographic model **m** is obtained by searching for the solution of the linear inverse problem:

$$\begin{pmatrix} \mathbf{G} \\ \alpha\mathbf{I} \\ \beta\mathbf{L} \end{pmatrix} \cdot \mathbf{m} = \begin{pmatrix} \mathbf{d} \\ 0 \\ 0 \end{pmatrix} \tag{2}$$

where the elements $G_{i,j}$ of the sensitivity matrix **G** contains the length of ray i in cell j, **I** is the identity matrix, **L** is the Laplace operator, α and β are respectively the damping and smoothing coefficients, and **d** is a vector containing the P traveltime residuals. The inversion is performed with the LSQR algorithm [*Paige and Saunders*, 1982]. The selection of damping and smoothing coefficients is based on a L curve criterion [*Hansen*, 1992]. Basically, in the overdamped/oversmoothed regime, a small increment of the regularization coefficients degrades significantly the misfit while in the underdamped/undersmoothed regime, decreasing the misfit requires introducing very strong complexities in the tomographic model. The L curve criterion looks for a combination of regularization parameters between these two extreme regimes, in order to find

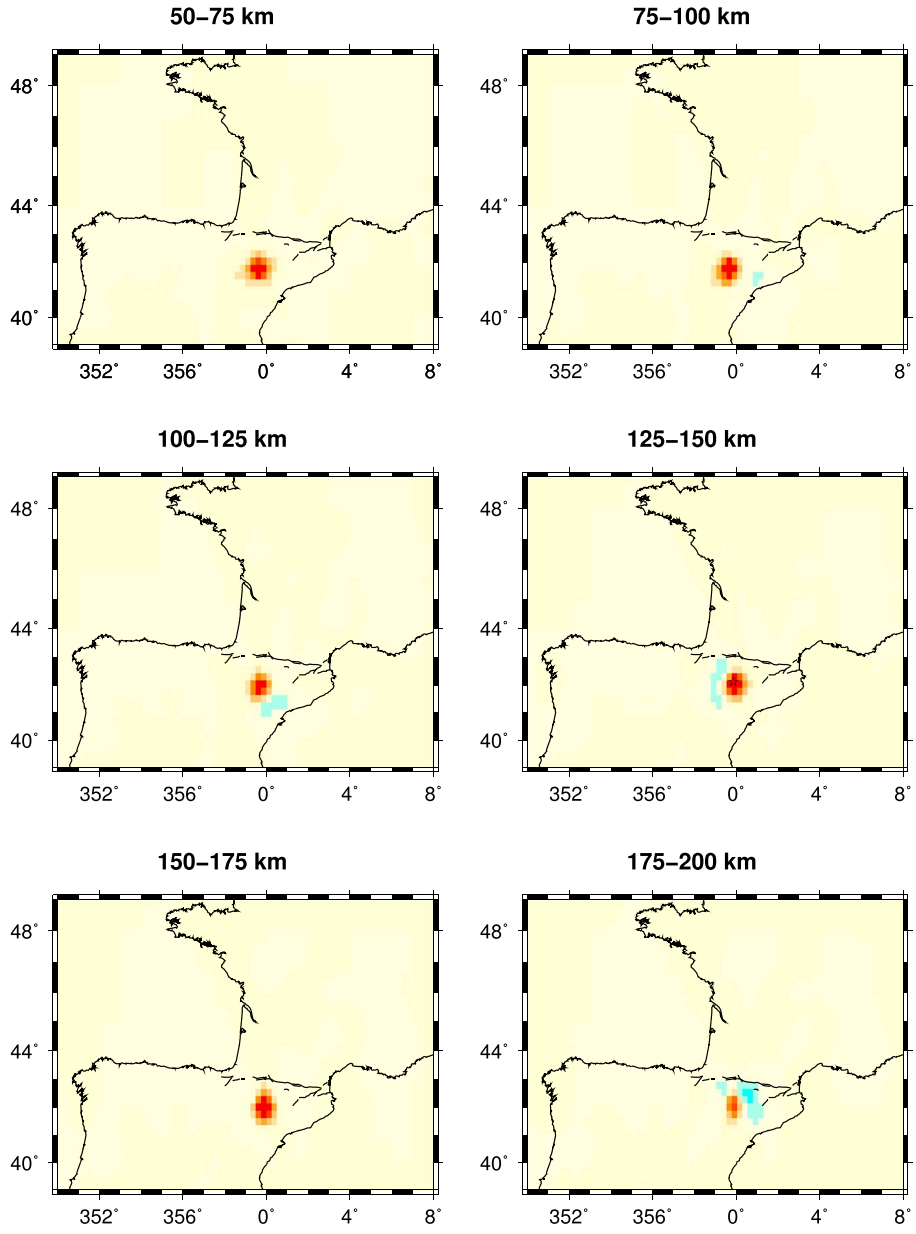

Figure 7. Results of the tomographic inversion obtained for a test model with a point-like anomaly located in the cell shown with the black star, between 125 and 150 km depth.

an acceptable compromise between model complexity and data misfit. For the chosen regularization coefficients, we obtain a variance reduction around 70% on the residuals corrected for ellipticity, station elevation, and crustal thickness. This rather large reduction of traveltime residuals is a strong indication of the quality of our data set.

5.2. Resolution

Assessing the spatial resolution of a tomographic model is an important problem in seismic tomography. In principle, this information is completely described by the resolution matrix, which can be explicitly derived and computed from the solution of the tomographic problem (2) that can be formally written

$$\tilde{\mathbf{m}} = \mathbf{A}^{-g} \cdot \mathbf{d} \tag{3}$$

where $\mathbf{A}^{-g}$ is the general inverse of the operator at the left-hand side of (2). Let us consider a test model $\mathbf{m}_{in}$, which predicts the traveltime residuals

$$\mathbf{d} = \mathbf{G} \cdot \mathbf{m}_{in} \tag{4}$$

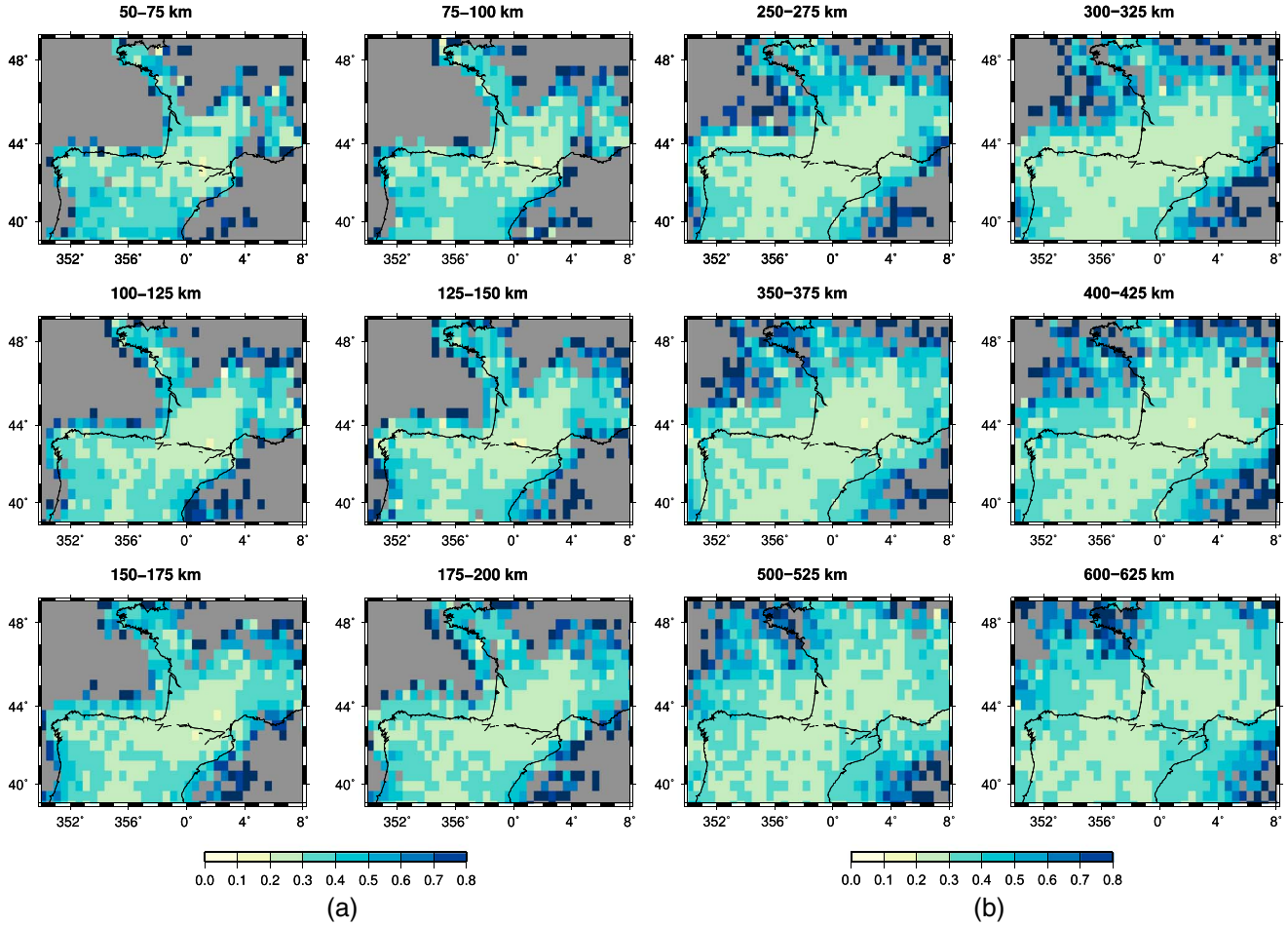

Figure 8. Lateral resolution (in degrees) in the tomographic grid (a) from 50 km to 200 km depth and (b) from 250 km to 625 km depth.

Inserting (4) into (3) leads to

$$\tilde{\mathbf{m}} = \mathbf{A}^{-g}\mathbf{G} \cdot \mathbf{m}_{in} = \mathbf{R} \cdot \mathbf{m}_{in} \tag{5}$$

where $\mathbf{R} = \mathbf{A}^{-g}\mathbf{G}$ is the resolution matrix. The resolution matrix represents the tomographic filter through which we can observe the interior of the Earth. For models described by a large number of free parameters M, the computation of the resolution matrix can be cumbersome. Here we exploit the property that the linear system (2) is solved extremely efficiently with the LSQR algorithm. This allows us to perform M independent inversions for M input spike models having a point-like anomaly in the different cells of the tomographic grid. Each inversion gives us a row of the resolution matrix. This algorithm leads to the same results as the direct computation of **R** [*Soldati et al.*, 2006] but for a fraction of the computational cost.

An example of the output of these inversions is presented in Figure 7. In this case, the test model was a point-like anomaly located in the cell shown with the black star, between 125 and 150 km depth. In the output model, which represents a row of the resolution matrix, this sharp feature has been spread both horizontally and vertically, but the effect of vertical smearing is stronger. Note also that the sign of the elements of the resolution matrix is sometimes negative, meaning that a positive velocity anomaly can produce an artificial negative velocity in the tomographic model. While such an image is very informative, it would be impractical to visualize and let alone store all the rows of the resolution matrix. A convenient way to extract and represent the resolution information contained in the resolution matrix is to determine its Gaussian approximation [*An*, 2012]. The idea is simply to fit a 2-D Gaussian at the depth of the input spike anomaly and to identify the horizontal resolution to the width of this Gaussian. Similarly, the vertical resolution can be estimated by fitting a 1-D Gaussian through a vertical profile constructed by taking the maximum value of the resolution matrix at each depth. This is certainly a crude approximation that cannot capture the full

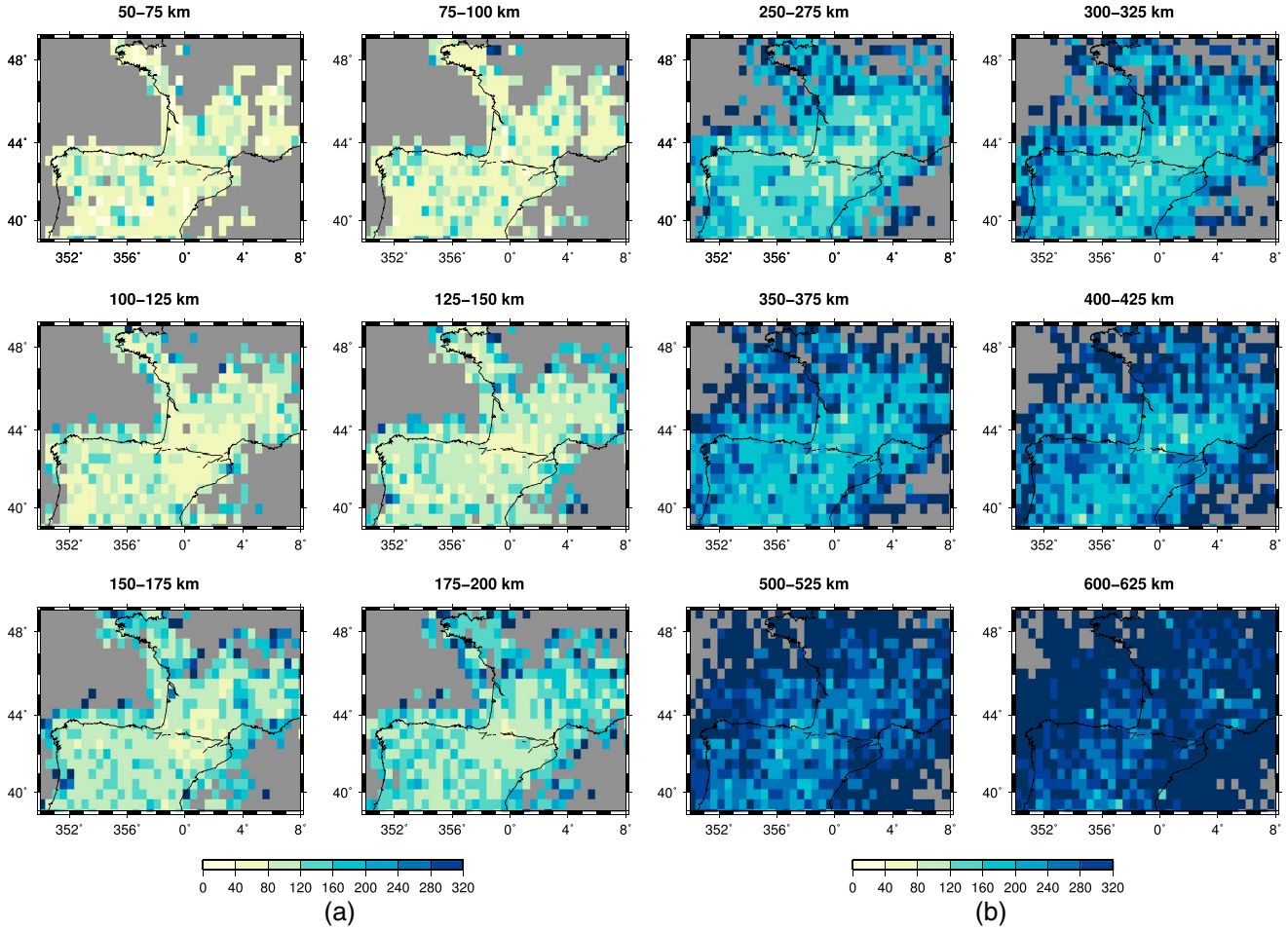

Figure 9. Vertical resolution (in kilometers) in the tomographic grid (a) from 50 km to 200 km depth and (b) from 250 km to 625 km depth.

complexity of the resolution kernel that can be seen on Figure 7 but which nevertheless provides some simple quantitative estimates of both lateral and vertical resolution in the tomographic model.

We have computed the full resolution matrix row-by-row by solving *M* spike test inverse problems with the LSQR algorithm and determined the Gaussian approximations of each output model. The lateral and vertical resolution in the tomographic model are shown in Figures 8 and 9, respectively. The best lateral resolution is found between 100 and 500 km depth and beneath the Pyrenees and Massif Central. The typical lateral resolution in the best resolved part of the model is around 0.25° which is the size of the cells in the tomographic grid. Resolution is much poorer along the vertical direction. The region where the vertical resolution is the largest is also found beneath the Pyrenees, which has the largest density of sensors and thus the best ray coverage. Beneath the Pyrenees, the vertical resolution is about 100 km between 100 and 200 km depth, but below 300 km depth, it rapidly degrades to values larger than 200 km. This lack of vertical resolution explains the well-known effect of vertical smearing in teleseismic tomography. It also emphasizes the importance of crustal corrections in order to avoid contaminating the deeper parts of the model by unaccounted for crustal structures. This is especially true for imaging structures beneath mountainous regions such as the Pyrenees, where strong and sharp lateral variations of crustal thickness are present.

5.3. Effects of Crustal Corrections

Including crustal corrections in addition to ellipticity and station elevation corrections improves the variance reduction by about 4%, which is quite significant. Figures 10 and 11 show the models obtained respectively without and with crustal corrections, from the surface down to 200 km depth. Significant differences are observed down to 200 km depth, in regions where crustal thickness is abnormally thick or thin, especially beneath the Pyrenees and Massif Central.

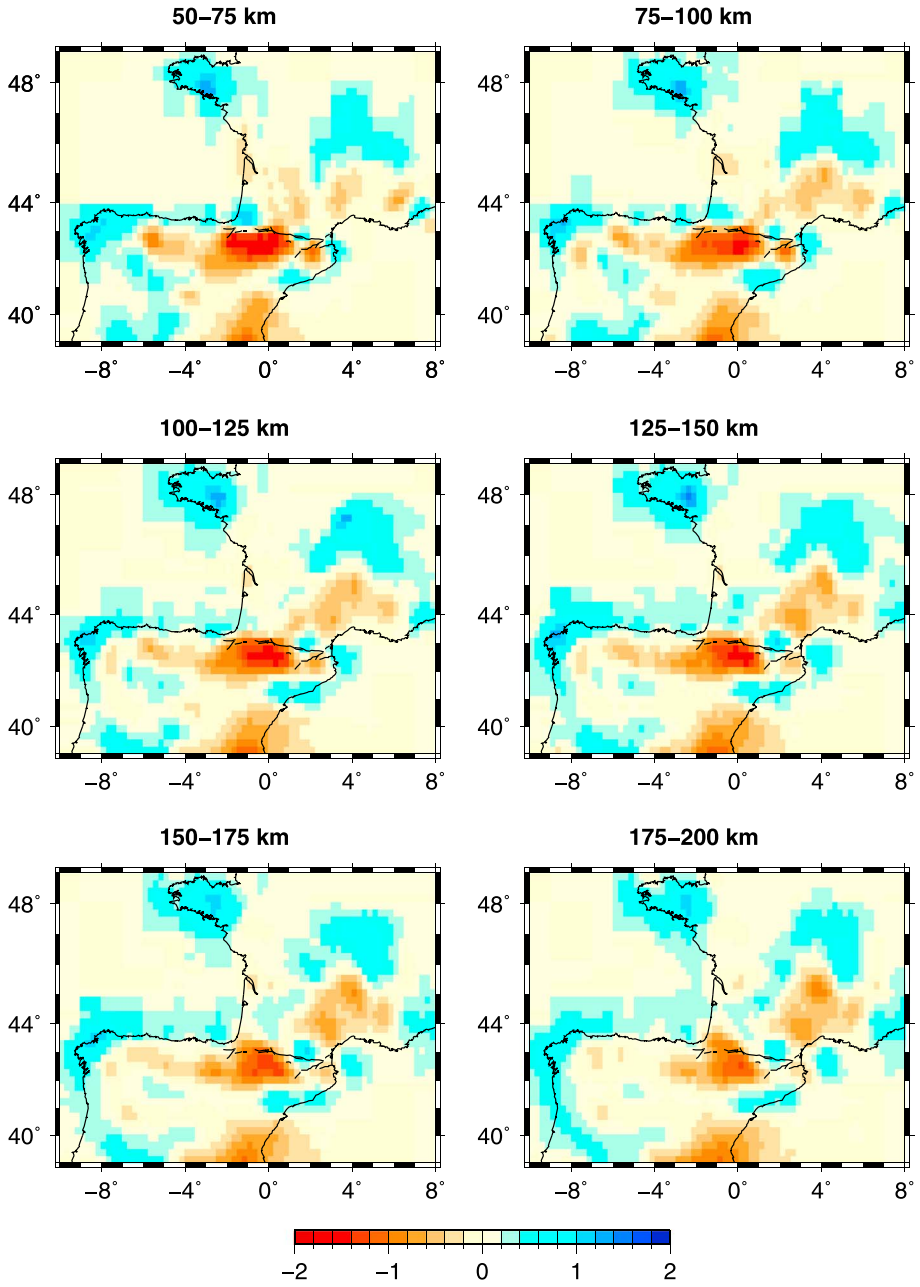

Figure 10. Map views of the *P* velocity model obtained without crustal corrections at 50, 75, 100, 125, 150, and 175 km depth. The color scale, in percents with respect to ak135 reference Earth model, is the same in all the plots.

6. Results

Figures 11 and 12 show map views and vertical cross sections of our regional tomographic model. Compared to previous models [e.g., *Souriau and Granet*, 1995; *Souriau et al.*, 2008; *Granet et al.*, 1995a, 1995b] the larger aperture of our seismological data set offers a much improved depth resolution but also allows us to observe the relations between lithospheric structures beneath the Pyrenees and Massif Central. In the following, we describe the main features observed in the tomographic model.

6.1. Massif Central

A broad slow velocity anomaly affects the lithosphere and asthenosphere of the Massif Central. This feature was already observed by *Granet et al.* [1995a] and *Granet et al.* [1995b], but owing to a broader aperture of our seismological array, its limits are now better defined. This anomaly has a sharp western boundary

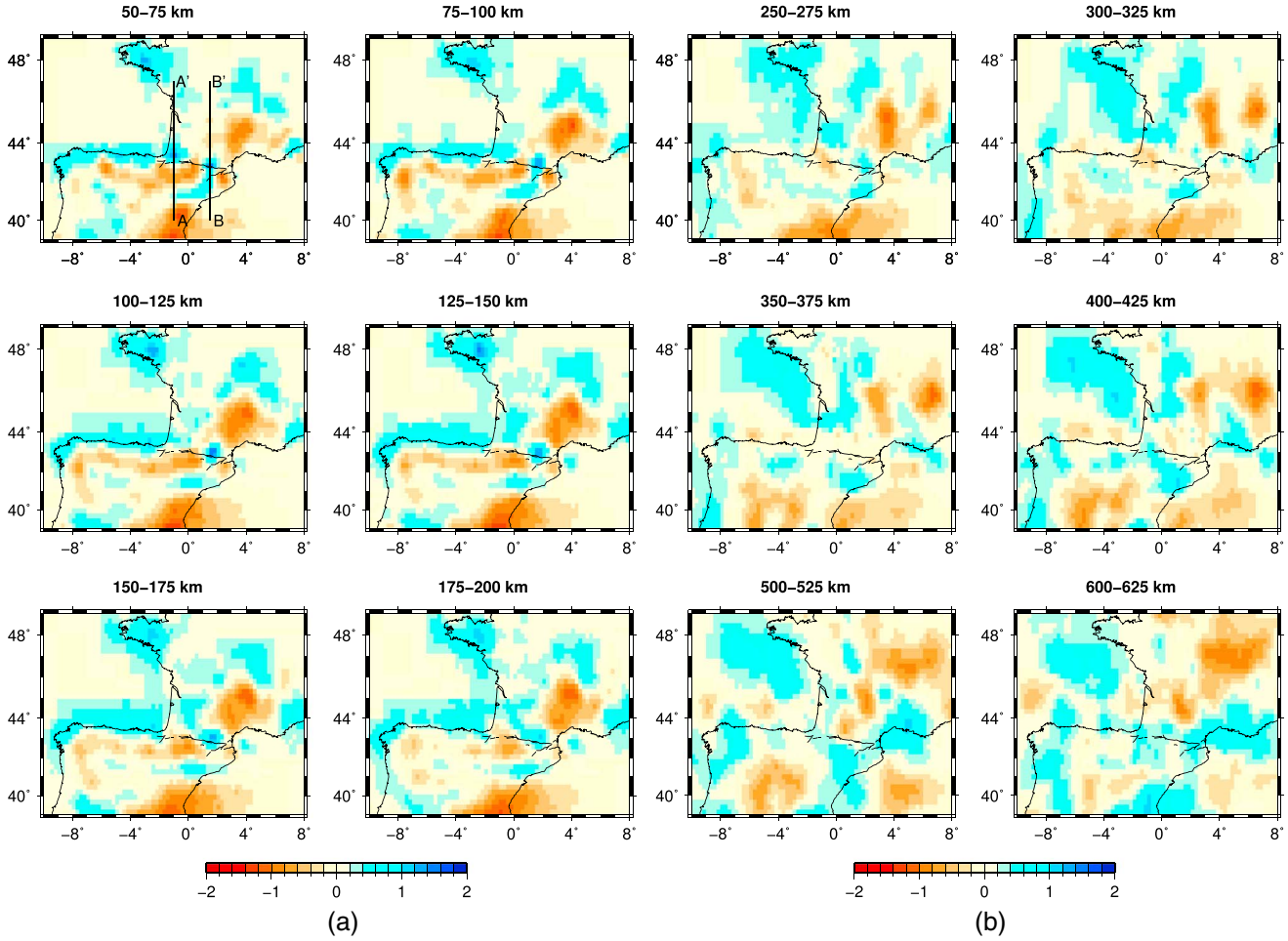

Figure 11. (a) Map views of the *P* velocity model obtained after crustal corrections at 50, 75, 100, 125, 150, and 175 km depth. (b) Map views of the model for *P* velocity anomalies at 250, 300, 350, 400, 500, and 600 km depth. The color scale, in percents with respect to the ak135 reference Earth model, is the same in all the plots.

that coincides with the Sillon Houiller (often also referred to as the "Toulouse Fault"), which seems to separate two distinct lithospheric domains with a sharp velocity contrast, the lithosphere of the Limousin being dominantly fast. The sharp boundary between the slow lithosphere of Massif Central and fast lithosphere of Limousin (west of the Sillon Houiller) is clearly expressed in the surface wave tomographic model of Europe obtained by *Zhu and Tromp* [2013]. A broad and pronounced low-velocity anomaly is also observed in the

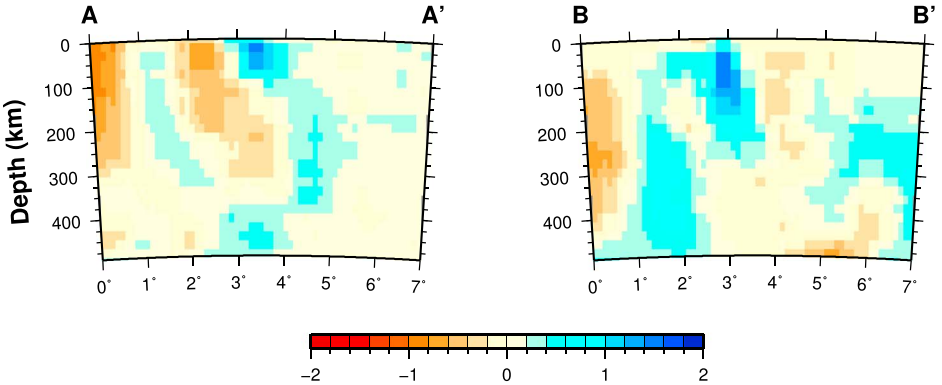

Figure 12. N-S vertical cross sections along longitudes (left) 1.0°W and (right) 1.5°E. The geometries of the two cross sections are shown in Figure 11.

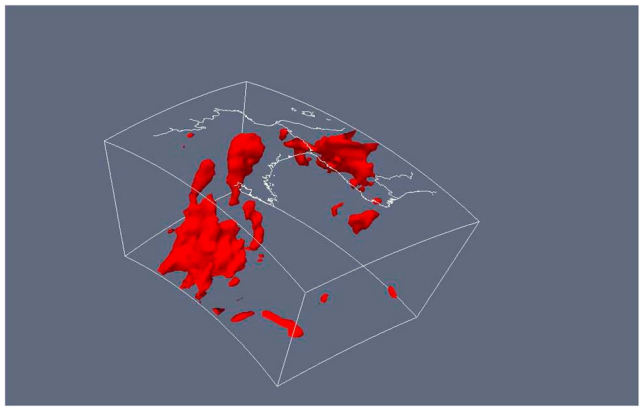

Figure 13. Three-dimensional view of the isocontour corresponding to a perturbation of −0.75% of the *P* velocity. The bottom of the box is at 900 km depth. The broad low-velocity anomaly in the transition zone is not connected from the shallow asthenospheric anomaly beneath the Massif Central.

transition zone to the northeast of the Massif Central. This deep anomaly does not seem to be connected to the shallow Massif Central anomaly (Figure 13). However, this cannot be completely excluded since this part of the model is poorly illuminated. It is possible that this deep anomaly is actually located deeper in the lower mantle and further to the northeast that is outside of our tomographic grid and that it is artificially mapped inside our regional model. If this is the case, this large slow anomaly could be related to the prominent deep lower mantle low-velocity anomaly under Central Europe imaged by global tomographic studies around 1000 km depth [e.g., *Goes et al.*, 1999].

6.2. Pyrenees

The most striking feature is the noncylindricity (along-strike variations) of the deep architecture of the Pyrenean domain. Indeed, lithospheric structures appear clearly segmented as can be seen in the map views of the model at lithospheric depth (125–150 km). While in the European lithosphere seismic velocities faster than in the Iberian lithosphere are generally observed, the limit between the fast and slow lithospheres does not follow the North Pyrenean Fault. This limit is found a few tens of kilometers north of the North Pyrenean Fault in the west, while it is a few tens of kilometers south in the east. The separation between these eastern and western domains approximately corresponds to the southern prolongation of the Toulouse Fault. The separation between a fast European lithosphere and a slow Iberian lithosphere shows another southward jump beneath the western Pyrenees and Basque Massifs, approximately coincident with the Pamplona Fault. The fast velocity anomaly is more pronounced beneath the east-central part of the range, between 50 and 200 km depth (section B-B′ in Figure 12). It is surrounded to the east and west by two low-velocity anomalies beneath the South Pyrenean Zone (SPZ). This fast anomaly is consistent with that imaged previously by *Souriau and Granet* [1995] and *Souriau et al.* [2008]. Another strong but shallower fast velocity anomaly is observed in the Labourd region (section A-A′ in Figure 12), which coincides with a pronounced positive Bouguer anomaly (Figure 14). At the eastern termination of the range low-velocities are observed, in particular beneath the Olot volcanic field. Below lithospheric depths ($z \geq 200$ km), no clear and coherent structures are observed. In particular, we note the absence of a deep pronounced high-velocity anomaly in the upper mantle and transition zone, which seems to rule out the presence of a detached oceanic lithosphere beneath the European plate.

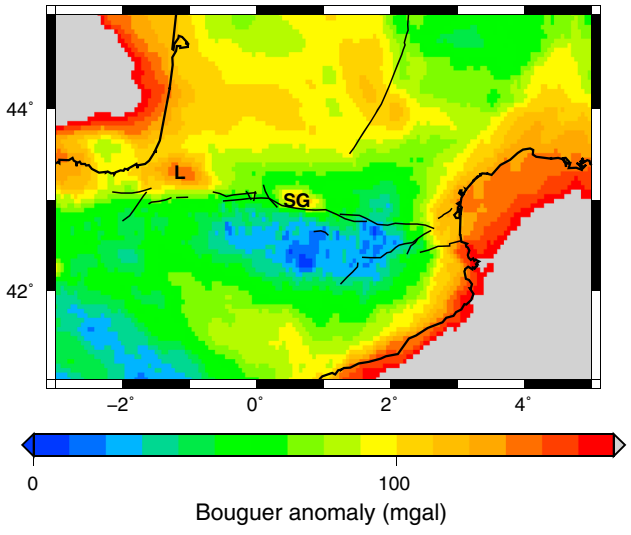

Figure 14. Map of Bouguer anomaly (in mGal), showing the Labourd (L) and Saint Gaudens (SG) positive anomalies.

6.3. Basque Massifs and the Cantabrians

To the north of the Cantabrian Mountains, from 8°W to 2°W, a shallow fast velocity anomaly is observed, which approximately follows the southern coast of the Bay of Biscay. This

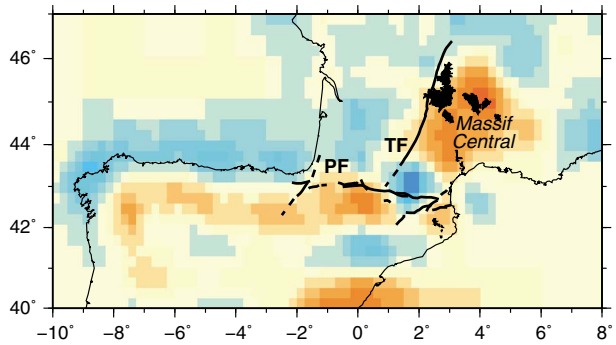

Figure 15. Map of *P* velocity anomalies between 125 and 150 km depth. The volcanic regions are the black shaded domains. The main faults in the Pyrenees are drawn with thin black solid lines while the Pamplona (PF) and Toulouse (TF) faults are drawn with thick black dashed lines.

anomaly is observed from 50 to 200 km depth. Its apparent width is about 100 km, but it could be larger since we cannot resolve its northern limit beneath the Bay of Biscay. A slow anomaly is also found in the same depth interval about 1° to the south that is almost parallel to the band of fast velocity. It connects to the slow anomaly that is observed in the western part of the South Pyrenean Zone.

6.4. Valencia Trough

A pronounced low-velocity anomaly is observed along the Catalan coast near Valencia between 100 and 300 km depth. This anomaly coincides with a significant crustal thinning documented by both deep seismic profiles and receiver functions (Figure 6). This slow anomaly extends toward the west in the Valencia Trough, an extensional basin that developed during late Oligocene-early Miocene, where it seems to continue down to the transition zone. However, the resolution is rather poor in this part of the model.

7. Discussion

7.1. Role of Reactivated Hercynian Structures During the Alpine Compression

The NE-SW segmentation of lithospheric structures observed in our tomographic images has important implications for discriminating the formation models of the Pyrenees. At the scales that are here well resolved in the tomographic images, of the order of a few tens of kilometers, two major faults can be identified (Figure15). These transverse faults oriented NE-SW were already identified as the main segmentation of a rift that affected the Armorican and Aquitaine margins during lower Cretaceous [*Boillot*, 1986; *Jammes et al.*, 2009]. Interestingly, these faults were first proposed on the basis of their disruptive effect on the basement of the Aquitaine margin, i.e., at crustal levels.

First, the Sillon Houiller clearly separates two distinct lithospheric domains beneath the Limousin and Massif Central. It can be seen that it has also a strong imprint on lithospheric structures further south in the Pyrenees, probably down to the North Pyrenean Zone (Figure 15). The Toulouse fault also seems to separate a western domain where strong positive Bouguer anomalies are found (the Labourd anomaly to the west and the Saint Gaudens anomaly in the western Central Pyrenees) from an eastern domain where such anomalies are absent [*Casas et al.*, 1997], as can be seen in Figure 14. The other major transfer zone, the Pamplona fault (sometimes named the Estella-Dax fault) is found to the west of the Pyrenees. It marks the western limit of the low-velocity anomaly in the lithosphere beneath the South Pyrenean Zone, which seems to be shifted toward the south to the west of the Pamplona fault. Wide-angle reflection profiles have confirmed the major influence of the Pamplona fault in the structuration of the crust [*Pedreira et al.*, 2003]. These profiles demonstrate that the Eurasian crust extends further southwest of the Pamplona fault, a result that has been confirmed and refined by a recent receiver function study in the western Pyrenees and Basque Massifs [*Diaz et al.*, 2012]. This implies that the crust and mantle lithosphere show similar offsets across the Pamplona fault, which clearly suggests that it is a major transfer zone that affects the whole lithosphere. Hence, these major inherited Hercynian faults controlled and localized the deformation during both the extensional rifting episode and the convergence.

The hypothesis of a rift affecting the Pyrenean domain before the onset of convergence has recently found further support. Indeed, the reexamination of the Lherz massif in eastern Pyrenees has led *Lagabrielle and Bodinier* [2008] to conclude that these mantle rocks were exhumed to the seafloor during Albian time before being reworked and deposited in Albian sediments. This requires extreme crustal thinning, as observed in deep magma-poor rifted margins like the Iberia-Newfoundland margins [*Jammes et al.*, 2009; *Lagabrielle et al.*, 2010]. The exposure of peridotites in the Pyrenees resulting from tectonic denudation of the mantle during Mesozoic rifting processes at a deep passive margin was already proposed by *Boillot* [1986]. Since the segmentation of the rift has a clear expression in the Pyrenean lithospheric architecture, this would suggest

that the E-W sinistral movement of Iberia with respect to Europe predates the rifting episode [*Jammes et al.*, 2009]. This idea was already proposed by *Souquet and Mediavilla* [1976] from a palinspastic reconstruction of the Pyrenees in the Mesozoic.

The role of the major NE-SW inherited transfer faults in the construction of the Pyrenees undermines the importance of the North Pyrenean Fault, which has been considered as the main structural boundary in the Pyrenees, often identified as the former plate boundary between Iberia and Europe [e.g., *Choukroune and Mattauer*, 1978]. This view is challenged by our tomographic model which shows little coherence between deep lithospheric structures beneath the Pyrenees and the trace of the North Pyrenean Fault at the surface.

7.2. Nature of the Velocity Anomalies Observed Beneath the Pyrenees

Velocity anomalies are produced by thermal anomalies and/or variations in composition or mineralogy, and it is not always easy to discriminate between these different sources of heterogeneities. If the two large low-velocity regions beneath the Massif Central and Valencia Trough are clearly related to thermal anomalies, the interpretation of the velocity anomalies observed in the Pyrenean lithosphere is less straightforward. Two localized high-velocity anomalies are predominant around 50 km depth (Figure 11). Vertical sections crossing these two anomalies are shown in Figure 12. The western anomaly (section A-A′) is the shallowest and disappears beneath 75 km depth. It coincides with the Labourd positive Bouguer anomaly (Figure 14) which, owing to the strong observed gradients, has been interpreted as a shallow isolated body of mantle material [*Casas et al.*, 1997]. Such a dense and presumably fast body is not captured by our crustal model, and it may very well explain the strong shallow velocity anomaly observed in our tomographic model. The more pronounced high-velocity anomaly observed beneath the eastern Pyrenees (section B-B′) is located east of the Saint Gaudens anomaly and has little expressed signature on the map of Bouguer anomalies. This would suggest a thermal origin for this seismic velocity anomaly located deeper in the European lithospheric mantle. A colder European lithosphere in central-eastern Pyrenees is consistent with a larger convergence to the east than to the west of the range, as proposed by *Teixell* [1998], among others. The contrasting thermal state of the lithosphere along the range may also be explained by a more intense Cretaceous extensional deformation to the west [*Boillot*, 1986; *Jammes et al.*, 2009], resulting in a subduction of a hotter Iberian lithosphere and a warmer lithospheric root. In any case, the lithospheric thickening of the European lithosphere is observable but moderate. This is in good agreement with the results of recent magnetotelluric profiles crossing the western and central Pyrenees that found that the European lithosphere is only 30 to 50 km thicker than the Iberian lithosphere [*Campanyà et al.*, 2012].

The last striking feature is the elongated slow anomaly in northern Spain. As already mentioned, it parallels a band of fast velocities that can be attributed to a cooler European lithosphere. Interestingly, both show a similar offset across the Pamplona Fault. As can be seen in section A-A′ (Figure 12), the slow velocities are relatively shallow and concentrated just beneath the Moho. It is very unlikely that this anomaly results from a thicker crust than considered in our crustal model, because the crustal thickness is very well constrained in this part of the model, from both numerous deep seismic sounding profiles and high-quality receiver function results. Such a shallow low-velocity anomaly could also be produced by very thick sedimentary basins, which have been indeed neglected in the computation of crustal corrections, but again the geometry of this anomaly does not seem to show a simple correlation with those of the Ebro and Duero basins. At this point, the origin of the low-velocity anomaly in the Iberian lithosphere remains enigmatic. However, its elongated and segmented geometry is reminiscent of a rift structure. Since Iberia experienced a northward displacement during the Alpine convergence, we may postulate that this anomaly is observed at the vertical of the region where rifting took place during Cretaceous. The slow velocities may thus have been produced by heating and metasomatism of the Iberian lithosphere by a hot and fluid-rich asthenospheric mantle.

7.3. Lithospheric Structures and Dynamics of the Pyrenees

The current tectonic regime in the Pyrenees is still uncertain and controversial but recent geodetic results suggest that the relative motion between Europe and Iberia is below 0.5 mm/yr (Nocquet and Calais, 2004). The vertical movements in the Pyrenees remain elusive, owing to the very small number of permanent GPS stations installed in the range and to their short operational period. In spite of currently undetectable horizontal movements, the Pyrenees are characterized by a moderate seismic activity [*Souriau and Pauchet*, 1998]. Another recent puzzling result is that all the significant recent earthquakes have focal mechanisms that indicate normal faulting with an extension direction approximately N-S, i.e., normal to the main axis of

the Pyrenees [*de Vicente et al.*, 2008; *Chevrot et al.*, 2011]. What causes this seismicity is still unclear [*Lacan and Ortuño*, 2012].

For the Alps, which present striking similarities with the Pyrenees, the current observed uplift has been interpreted as a consequence of passive unloading due to erosion [*Champagnac et al.*, 2009]. Numerical models of erosion-induced deformation have shown that this is a viable mechanism to produce extensional deformations in a mountain range, even if it experiences a moderate amount of shortening [*Vernant et al.*, 2013]. While this may provide an appealing explanation for the dynamics of the Alps, such a mechanism is difficult to reconcile with some basic observations that have been made in the Pyrenees. First, erosion-driven deformations would produce extension only in the elevated part of the mountain range. However, we observe extension in the foothills of the Pyrenees as far north as the gas field of Lacq, for example, where the 2 September 2013 magnitude 4.0 event had a clear normal fault focal mechanism (B. Delouis, personal communication, 2013). Second, erosion reduces crustal thickness, and in the absence of any other influences, the surface is expected to move downward [*England and Molnar*, 1990]. In the Pyrenees, and in particular, in the Eastern Pyrenees, we observe just the opposite [*Gunnell et al.*, 2008], and in the central part of the Pyrenees, the topography is still overcompensated by a very thick crust. In addition, east of 1°E, a Pyrenean peneplain has been uplifted by about 2 km during the last 12 Ma [*Gunnell et al.*, 2009]. The preservation of this low-relief topography implies that denudation rates have remained very low, which also rules out any strong influence of exhumation, at least in this part of the range. To explain this uplift, *Gunnell et al.* [2008] advocate the thermal erosion of the lithospheric root that started around 12 Ma and which also produced the extensional basins in the eastern Pyrenees and triggered volcanism in the Banyoles-Olot region around 10 Ma. The heat source that consumed the lithosphere to the east of the Pyrenees may have come from the rollback of the Tethian slab during the opening of the Algero-Provençal basin, which promoted a return asthenospheric flow from the Massif Central [*Gunnell et al.*, 2008; *Barruol and Granet*, 2002]. This is broadly consistent with our tomographic model, which shows a low-velocity anomaly to the east of the Pyrenees that seems to be connected to the slow anomaly beneath the Massif Central.

Numerical modeling of crustal deformations have shown that the flexural thickening of the European and Iberian crusts cannot be reproduced without a subduction load, produced by a negatively buoyant subducted slab [*Beaumont et al.*, 2000]. If this load was still present, it would produce regional compressive stresses [*Fleitout and Froidevaux*, 1982]. Since seismicity shows that the Pyrenees are in extension, this would suggest that the lithospheric root has already disappeared or is still being consumed by slowly warming up, producing uplift and extension in the overlying lithosphere [*Brunet*, 1986; *Fleitout and Froidevaux*, 1982]. The latter would be consistent with the rather moderate fast velocity anomalies present in the European lithosphere.

7.4. General Lessons Learned for Regional Tomography

The regional tomography of the Pyrenees has clearly demonstrated the importance of crustal corrections to image properly the velocity anomalies in the lithosphere and asthenosphere. However, the computation of accurate crustal corrections requires a very detailed crustal model. An initial crustal model constructed from the analysis of receiver functions only was found very insufficient, producing large artifacts in the tomographic model. The main problem was the poor spatial resolution of the crustal model that had to be interpolated between rather distant seismological stations. While the PYROPE and IBERARRAY deployments are characterized by a density of sensors that compares favorably even with the higher standards, the USArray having a typical interstation distance of about 70 km compared to about 60 km for the PYROPE experiment, this density is still not sufficient in mountain ranges such as the Pyrenees, where crustal structure is very heterogeneous and can vary strongly over very short distances. To make things worse, it was extremely difficult (but most often simply impossible) to constrain the Moho depth below the stations installed in the foreland Ebro and Aquitaine basins, owing to strong reverberations in the sedimentary layers that masked conversions on deeper interfaces, but also below the stations installed in the axial zone, owing to very complicated receiver functions showing a strong variability with azimuth. Therefore, the crustal model built from receiver functions had a much coarser resolution in the Pyrenees and surrounding regions, precisely where the finest resolution is required. In our study, the compilation of the results obtained from reflection and refraction profiles brought crucial constraints on the variations of crustal thickness in the Pyrenees. We believe that it would have been actually impossible to obtain a reliable crustal model without them. In principle, surface waves can also be used to constrain crustal structure, and they have been sometimes successfully exploited in addition to body waves in regional tomographic studies [e.g., *Obrebski et al.*,

2011], but their potential to resolve lateral and vertical variations in the crust remains rather limited. When considering empirical Green's functions in ambient noise tomography, only short periods ($T \leq 25$ s) can be reliably obtained from noise recorded by small-aperture arrays, which will make the determination of the Moho depth problematic. Therefore, the most reasonable approach is probably to be pragmatic, by trying to incorporate into the inversion any a priori information we can get about the crust.

Another important ingredient in our tomographic study was the very high quality of the traveltime picks that exploited the similarity of a teleseismic wave on the records of a seismological array with a regional aperture. We believe that the importance of the quality of the traveltime data set and of crustal corrections far outweighs the importance of finite-frequency effects in the results of regional tomography, at least for the lithosphere and upper mantle. Finite-frequency effects may become important at larger depth. However, to properly resolve the deeper parts of the model it may be also important to embed the regional grid inside a global tomographic grid [e.g., *Widiyantoro and van der Hilst*, 1997], or simply to solve a global tomographic problem in order to avoid mapping structures that are located outside the tomographic grid inside the regional tomographic model.

8. Conclusions

Our regional *P* wave tomographic model obtained from the exploitation of the data of the PYROPE and IBERARRAY temporary experiments provides high-resolution images of lithospheric and sublithospheric structures beneath the Pyrenees and Massif Central. The notable features of our tomographic study are the quality of absolute and relative *P* traveltime measurements obtained by waveform similarity, and the accurate crustal corrections computed into a new detailed crustal model constructed from a compilation of seismic reflection/refraction profiles and of receiver functions.

Thanks to the high density of seismological sensors, especially in the Pyrenees, the lateral resolution in our model is of the order of 25 km at 100 km depth, but the vertical resolution is much poorer. The slow anomaly beneath Massif Central reflects lithospheric thinning and asthenosphere upwelling. Another strong low-velocity anomaly is also observed beneath the Valencia Trough, certainly related to a strong thermal anomaly that is also well documented. The absence of a pronounced fast anomaly coherent along the whole Pyrenean range rules out the subduction of an oceanic domain below the European plate during the convergence. Rather, the Pyrenean lithospheric architecture appears segmented by the Pamplona and Toulouse faults, two major vertical translithospheric shear zones. These Hercynian structures were first reactivated during the Mesozoic rifting and later during the Cenozoic convergence. This is a clear indication of the strong influence of inheritance on the tectonic evolution of the Pyrenean domain. To conclude, our tomographic model brings additional support to the idea that the Pyrenees were produced by the inversion of a segmented rift that was buried by subduction beneath the European plate.

The new structural model of the Pyrenees, together with the recently published new evidences for rifting in the Pyrenean domain during the Albian/Aptian, provides crucial constraints for the formation of the Pyrenees and calls for a more detailed confrontation of tomographic images with geological data.

Acknowledgments

The PYROPE experiment was supported by the French Research Agency ANR blanc program (project PYROPE, ANR-09-BLAN-0229). We also acknowledge SISMOB, the French seismic mobile pool (a component of the RESIF consortium), for providing us with the seismological instrumentation for the temporary deployments. We also thank the IGN and IGC for making their broadband data available to us, Julie Perrot for sending us data from a short-period array in Vendee and Jean Michel Douchain for preparing the data of the ReNass stations in the Massif Central. This is a contribution of the Team Consolider-Ingenio 2010 TOPO-IBERIA (CSD2006-00041).

References

Aki, K., A. Christofferson, and E. S. Husebye (1977), Determination of the three-dimensional seismic structures of the lithosphere, *J. Geophys. Res.*, *82*, 277–296.

An, M. (2012), A simple method for determining the spatial resolution of a general inverse problem, *Geophys. J. Int.*, *191*, 849–864.

Barruol, G., and M. Granet (2002), A Tertiary asthenospheric flow beneath the southern Massif Central indicated by upper mantle seismic anisotropy and related to the west Mediterranean extension, *Earth Planet. Sci. Lett.*, *202*, 31–47.

Bassin, C., G. Laske, and G. Masters (2000), The current limits of resolution for surface wave tomography in North America, *EOS Trans. AGU*, *81*, F897, Fall Meet. Suppl.

Beaumont, C., J. A. Muñoz, J. Hamilton, and P. Fullsak (2000), Factors controlling the Alpine evolution of the central Pyrenees inferred from a comparison of observations and geodynamical models, *J. Geophys. Res.*, *105*, 8121–8145.

Boillot, G. (1986), Comparison between the Galicia and Aquitaine margins, *Tectonophysics*, *129*, 243–255.

Bronner, A., D. Sauter, G. Manatschal, G. Péron-Pinvidic, and M. Munschy (2011), Magmatic breakup as an explanation for magnetic anomalies at magma-poor rifted margins, *Nat. Geosci.*, *4*, 549–553.

Bronner, A., D. Sauter, G. Manatschal, G. Péron-Pinvidic, and M. Munschy (2012), Reply: Problematic plate reconstruction, *Nat. Geosci.*, *5*, 677.

Brunet, M. F. (1986), The influence of the evolution of the Pyrenees on adjacent basins, *Tectonophysics*, *129*, 343–354.

Burg, J. P., J. P. Brun, and J. van den Driessche (1990), Le Sillon Houiller du Massif Central français: Faille de trasnfert pendant l'amincissement crustal de la chaîne varisque?, *C. R. Acad. Sci.*, *311*, 147–152.

Campanyà, J., J. Ledo, P. Queralt, A. Marcuello, M. Liesa, and J. A. Muñoz (2012), New geoelectrical characterisation of a continental collision zone in the West-Central Pyrenees: Constraints from long-period and broadband magnetotellurics, *Earth Planet. Sci. Lett.*, *333-334*, 112–121.

Casas, A., P. Kearey, L. Rivero, and C. R. Adam (1997), Gravity anomaly map of the Pyrenean region and a comparison of the deep geological structure of the western and eastern Pyrenees, *Earth Planet. Sci. Lett.*, *150*, 65–78.

Champagnac, J. D., F. Schlunegger, K. Norton, F. von Blanckenburg, L. M. Abbuhl, and M. Schwab (2009), Erosion-driven uplift of the modern Central Alps, *Tectonophysics*, *474*, 236–249.

Chevrot, S. (2002), Optimal measurement of relative and absolute delay times by simulated annealing, *Geophys. J. Int.*, *151*, 164–171.

Chevrot, S., and R. van der Hilst (2000), The poisson ratio of the Australian crust: Geological and geophysical implications, *Earth Planet. Sci. Lett.*, *183*, 121–132.

Chevrot, S., M. Sylvander, and B. Delouis (2011), A preliminary catalogue of moment tensors for the pyrenees, *Tectonophysics*, *510*, 239–251.

Choukroune, P., and M. Mattauer (1978), Tectonique des plaques et Pyrénées: Sur le fonctionnement de la faille transformante nord-pyrénéenne; comparaison avec des modèles actuels, *Bull. Soc. Geol. Fr.*, *7*, 689–700.

Choukroune, P., and the ECORS team (1989), The ECORS pyrenean deep seismic profile reflection data and the overall structure of an orogenic belt, *Tectonics*, *8*, 23–39.

Daignières, M., J. Gallart, E. Banda, and A. Hirn (1982), Implications of the seismic structure for the orogenic evolution of the Pyrenean range, *Earth Planet. Sci. Lett.*, *57*, 88–100.

Daignières, M., B. de Cabissole, J. Gallart, A. Hirn, E. Surinach, and E. Torne (1989), Geophysical constraints on the deep structure along the ECORS Pyrenees line, *Tectonics*, *8*, 1051–1058.

de Vicente, G., S. Cloetingh, A. Muñoz Martin, A. Olaiz, D. Stich, R. Vegas, J. Galindo-Zaldivar, and J. Fernández-Lozano (2008), Inversion of moment tensor focal mechanisms for active stresses around the microcontinental Iberia: Tectonic implications, *Tectonics*, *27*, TC1009, doi:10.1029/2006TC002093.

Diaz, J., and J. Gallart (2009), Crustal structure beneath the Iberian Peninsula and surrounding waters: A new compilation of deep seismic sounding results, *Phys. Earth Planet. Inter.*, *173*, 181–190.

Diaz, J., D. Pedreira, M. Ruiz, J. A. Pulgar, and J. Gallart (2012), Mapping the indentation between the Iberian and Eurasian plates beneath the Western Pyrenees/Eastern Cantabrian Mountains from receiver function analysis, *Tectonophysics*, *570-571*, 114–122.

ECORS Pyrenees Team (1988), The ECORS deep reflection seismic survey across the Pyrenees, *Nature*, *331*, 508–511.

England, P. C., and P. Molnar (1990), Surface uplift, uplift of rocks, and exhumation of rocks, *Geology*, *18*, 1173–1177.

Fleitout, L., and C. Froidevaux (1982), Tectonics and topography for a lithosphere containing density heterogeneities, *Tectonics*, *1*, 21–56.

Gallart, J., M. Daignières, E. Banda, E. Surinach, and A. Hirn (1980), The Eastern Pyrenean domain: Lateral variations at crust-mantle level, *Ann. Geophys.*, *36*, 457–480.

Goes, S., W. Spakman, and H. Bijwaard (1999), A lower mantle source for central european volcanism, *Science*, *286*, 1928–1931.

Gómez-Ortiz, D., B. N. P. Agarwal, R. Tejero, and J. Ruiz (2011), Crustal structure from gravity signatures in the Iberian Peninsula, *Geol. Soc. Am. Bull.*, *123*, 1247–1257.

Granet, M., G. Stoll, J. Dorel, U. Achauer, G. Poupinet, and K. Fuchs (1995a), Massif Central (France): New constraints on the geodynamical evolution from teleseismic tomography, *Geophys. J. Int.*, *121*, 33–48.

Granet, M., M. Wilson, and U. Achauer (1995b), Imaging a mantle plume beneath the French Massif Central, *Earth Planet. Sci. Lett.*, *136*, 281–296.

Gunnell, Y., H. Zeyen, and M. Calvet (2008), Geophysical evidence of a missing lithospheric root beneath the Eastern Pyrenees: Consequences for post-orogenic uplift and associated geomorphic signatures, *Earth Planet. Sci. Lett.*, *276*, 302–313.

Gunnell, Y., M. Calvet, S. Brichau, A. Carter, J. P. Aguilar, and H. Zeyen (2009), Low long-term erosion rates in high-energy mountain belts: Insights from thermo- and biochronology in the Eastern Europe, *Earth Planet. Sci. Lett.*, *278*, 208–218.

Hansen, P. C. (1992), Analysis of discrete ill-posed problems by means of the L-curve, *SIAM Rev.*, *34*, 561–580.

Jammes, S., G. Manatschal, L. Lavier, and E. Masini (2009), Tectonosedimentary evolution related to extreme crustal thinning ahead of a propagating ocean: Example of the western Pyrenees, *Tectonics*, *28*, TC4012, doi:10.1029/2008TC002406.

Kennett, B. L. N., E. R. Engdahl, and R. Buland (1995), Constraints on seismic velocities in the Earth from traveltimes, *Geophys. J. Int.*, *122*, 108–124.

Kirkpatrick, S., C. D. Gelatt, and M. P. Vecchi (1983), Optimization by simulated annealing, *Science*, *220*, 671–680.

Knuth, D. E. (1968), *The Art of Computer Programming*, Addison-Wesley, Reading, Mass.

Lacan, P., and M. Ortuño (2012), Active tectonics of the Pyrenees: A review, *J. Iber. Geol.*, *38*, 9–30.

Lagabrielle, Y., P. Labaume, and M. de Saint Blanquat (2010), Mantle exhumation, crustal denudation, and gravity tectonics during Cretaceous rifting in the Pyrenean realm (SW Europe): Insights from the geological setting of the lherzolite bodies, *Tectonics*, *29*, TC4012, doi:10.1029/2009TC002588.

Lagabrielle, Y., and J. L. Bodinier (2008), Submarine reworking of exhumed subcontinental mantle rocks: Field evidence from the Lherz peridotites, French Pyrenees, *Terra Nova*, *20*, 11–21.

Le Pichon, X., J. Bonnin, and J. C. Sibuet (1970), La faille nord-pyrénéenne: Faille transformante liée à l'ouverture du golfe de Gascogne, *C. R. Acad. Sci., Ser.*, *271*, 1941–1944.

Le Pichon, X., J. Bonnin, J. Francheteau, and J. C. Sibuet (1971), Une hypothèse d'évolution tectonique du Golfe de Gascogne, in *Histoire Structurale du Golfe de Gascogne*, edited by J. Debysier, X. Le Pichon, and M. Montadert, pp. 1–44, Technip, Paris, France.

Li, C., R. D. van der Hilst, and M. N. Toksoz (2006), Constraining P-wave velocity variations in the upper mantle beneath Southeast Asia, *Phys. Earth Planet. Inter.*, *154*, 180–195.

Ligorria, J. P., and C. J. Ammon (1999), Iterative deconvolution and receiver-function estimation, *Bull. Seismol. Soc. Am.*, *89*, 1395–1400.

McCaig, A. M. (1988), Deep geology of the Pyrenees, *Nature*, *331*, 480–481.

Muñoz, J. A. (1992), Evolution of a continental collision belt: ECORS-Pyrenees crustal balanced section, in *Thrust Tectonics*, edited by K. R. McClay, pp. 235–246, Chapman and Hall, London, U. K.

Obrebski, M., R. M. Allen, F. Pollitz, and S.-H. Hung (2011), Lithosphere-asthenosphere interaction beneath the western United States from the joint inversion of body-wave traveltimes and surface-wave phase velocities, *Geophys. J. Int.*, *185*, 1003–1021.

Paige, C. C., and M. A. Saunders (1982), LSQR: An algorithm for sparse linear equations and sparse least squares, *ACM Trans. Math. Softw.*, *8*, 43–71.

Pedreira, D., J. A. Pulgar, J. Gallart, and J. Diaz (2003), Seismic evidence of Alpine crustal thickening and wedging from the western Pyrenees to the Cantabrian Mountains (north Iberia), *J. Geophys. Res.*, *108*(B4), 2204, doi:10.1029/2001JB001667.

Perrier, G., and J. C. Ruegg (1973), Structure profonde du Massif Central français, *Ann. Geophys.*, *29*, 435–502.

Roure, F., et al. (1989), ECORS deep seismic data and balanced cross sections: Geometric constraints on the evolution of the Pyrenees, *Tectonics*, *8*, 41–50.
Sapin, M., and A. Hirn (1974), Results of explosion seismology in the Southern Rhone Valley, *Ann. Geophys.*, *30*, 181–202.
Sapin, M., and C. Prodehl (1973), Long range profiles in western Europe I—Crustal structure between the Bretagne and the Central Massif of France, *Ann. Geophys.*, *29*, 127–145.
Sibuet, J. C., S. P. Srivastava, and W. Spakman (2004), Pyrenean orogeny and plate kinematics, *J. Geophys. Res.*, *109*, B08104, doi:10.1029/2003JB002514.
Soldati, G., L. Boschi, and A. Piersanti (2006), Global seismic tomography and modern parallel computers, *Ann. Geophys.*, *49*, 977–986.
Souquet, P., and F. Mediavilla (1976), Nouvelle hypothèse sur la formation des pyrénées, *C. R. Acad. Sci.*, *282*, 2139–2142.
Souriau, A., and M. Granet (1995), A tomographic study of the lithosphere beneath the pyrenees from local and teleseismic data, *J. Geophys. Res.*, *100*, 18,117–18,134.
Souriau, A., and H. Pauchet (1998), A new synthesis of Pyrenean seismicity and its tectonic implications, *Tectonophysics*, *290*, 221–244.
Souriau, A., S. Chevrot, and C. Olivera (2008), A new tomographic image of the pyrenean lithosphere from teleseismic data, *Tectonophysics*, *460*, 206–214.
Spakman, W., and H. Bijwaard (2001), Optimization of cell parameterizations for tomographic inverse problems, *Pure Appl. Geophys.*, *158*, 1401–1423.
Srivastava, S. P., J. C. Sibuet, S. Cande, W. R. Roest, and I. D. Reid (2000), Magnetic evidence for slow seafloor spreading during the formation of the Newfoundland and Iberian margins, *Earth Planet. Sci. Lett.*, *182*, 61–76.
Tapponnier, P. (1977), Evolution tectonique du système alpin en Méditerranée: Poinçonnement et écrasement rigide-plastique, *Bull. Soc. Geol. Fr.*, *29*, 437–460.
Teixell, A. (1998), Crustal structure and orogenic material budget in the west central Pyrenees, *Tectonics*, *3*, 395–406.
Torné, M., B. De Cabissole, R. Bayer, A. Casas, M. Daignières, and A. Rivero (1989), Gravity constraints on the deep structure of the pyrenean belt along the ECORS profile, *Tectonophysics*, *165*, 105–116.
Tucholke, B. E., and J. C. Sibuet (2012), Comment: Problematic plate reconstructions, *Nat. Geosci.*, *5*, 676–677.
Vacher, P., and A. Souriau (2001), A 3-D model of the Pyrenean deep structure based on gravity modelling, seismic images, and petrological constraints, *Geophys. J. Int.*, *145*, 460–470.
van der Voo, R. (1969), Paleomagnetic evidence for the rotation of the Iberian Peninsula, *Tectonophysics*, *7*, 5–56.
VanDecar, J. C., and R. S. Crosson (1990), Determination of teleseismic relative phase arrival times using multi-channel cross-correlation and least squares, *Bull. Seismol. Soc. Am.*, *80*, 150–169.
Vernant, P., F. Hivert, J. Chéry, P. Steer, R. Cattin, and A. Rigo (2013), Erosion-induced isostatic rebound triggers extension in low convergent mountain ranges, *Geology*, *41*, 467–470.
Vissers, R. L. M., and P. T. Meijer (2012), Mesozoic rotation of Iberia: Subduction in the pyrenees?, *Earth Sci. Rev.*, *110*, 93–110.
Waldhauser, F., R. Lippitsch, E. Kissling, and J. Ansorge (2002), High-resolution teleseismic tomography of upper-mantle structure using an a priori three-dimensional crustal model, *Geophys. J. Int.*, *150*, 403–414.
Widiyantoro, S., and R. D. van der Hilst (1997), Mantle structure beneath Indonesia inferred from high-resolution tomographic imaging, *Geophys. J. Int.*, *130*, 167–182.
Zhu, H., and J. Tromp (2013), Mapping tectonic deformation in the crust and upper mantle beneath Europe and the North Atlantic Ocean, *Science*, *341*, 871–875.
Ziegler, P. A. (1992), European Cenozoic rift system, *Tectonophysics*, *208*, 91–111.
Ziegler, P. A., and P. Dèzes (2006), *Crustal Evolution of Western and Central Europe*, vol. 32, pp. 43–56, Geol. Soc. London, Mems., doi:10.1144/GSL.MEM.2006.032.01.03.